HHS Public Access

Author manuscript

Neurobiol Dis. Author manuscript; available in PMC 2022 May 04.

Published in final edited form as:

Neurobiol Dis. 2021 September ; 157: 105431. doi:10.1016/j.nbd.2021.105431.

Neonatal stroke enhances interaction of microglia-derived extracellular vesicles with microglial cells

Matthieu Lecuyer, **Praneeti Pathipati**, **Joel Faustino**, **Zinaida S. Vexler***

Department of Neurology, UCSF, San Francisco, CA, USA

Abstract

Microglial cells support brain homeostasis under physiological conditions and modulate brain injury in a context-dependent and brain maturation-dependent manner. Microglial cells protect neonatal brain from acute stroke. While microglial signaling via direct cell-cell interaction and release of variety of molecules is intensely studied, less is known about microglial signaling via release and uptake of extracellular vesicles (EVs). We asked whether neonatal stroke alters release of microglial EVs (MEV) and MEV communication with activated microglia. We pulled down and plated microglia from ischemic-reperfused and contralateral cortex 24 h after transient middle cerebral artery occlusion (tMCAO) in postnatal day 9 mice, isolated and characterized microglia-derived microvesicles (P3-MEV) and exosomes (P4-MEV), and determined uptake of fluorescently labeled P3-MEV and P4-MEV by plated microglia derived from ischemic-reperfused and contralateral cortex. We then examined how reducing EVs release in neonatal brain—by intra-cortical injection of CRISPR-Cas9-Smpd3/KO (Smpd3/KD) to downregulate Smpd3 gene to disrupt neutral sphingomyelinase-2 (N-SMase2)—impacts P3-MEV and P4-MEV release and stroke injury. Both size and protein composition differed between P3-MEV and P4-MEV. tMCAO further altered protein composition of P3-MEV and P4-MEV and significantly, up to 5-fold, increased uptake of both vesicle subtypes by microglia from ischemic-reperfused regions. Under physiological conditions neurons were the predominant cell type expressing N-SMase-2, an enzyme involved in lipid signaling and EVs release. After tMCAO N-SMase-2 expression was diminished in injured neurons but increased in activated microglia/macrophages, leading to overall reduced N-SMase-2 activity. Compared to intracerebral injection of control plasmid, CRISPR-Cas9-Smpd3/Ct, Smpd3/KD injection further reduced N-SMase-2 activity and significantly reduced injury. Smpd3 downregulation decreased MEV release from injured regions, reduced Smpd3/KD-P3-MEV uptake and abolished Smpd3/KD-P4-MEV uptake by microglia from ischemic-reperfused region. Cumulatively, these data demonstrate that microglial cells release both microvesicles and exosomes in naïve neonatal brain, that the state of microglial

*Corresponding author at: University California San Francisco, Department of Neurology, 675 Nelson Rising Lane, San Francisco, CA 94158-0663, USA. Zena.Vexler@ucsf.edu (Z.S. Vexler).

Author statement

ML – Data curation; Formal analysis; Investigation; Writing - original draft; Writing - review & editing.

PP – Data curation; Investigation; Methodology; Writing - original draft; Writing - review & editing.

JF – Data curation; Formal analysis; Methodology; Writing - original draft; Writing - review & editing

ZSV - Conceptualization; Data curation; Formal analysis; Funding acquisition; Investigation; Project administration; Writing - original draft; Writing - review & editing

Appendix A. Supplementary data

Supplementary data to this article can be found online at https://doi.org/10.1016/j.nbd.2021.105431.

activation determines both properties of released EVs and their recognition/uptake by microglia in ischemic-reperfused and control regions, suggesting a modulatory role of MEV in neonatal stroke, and that sphingosine/N-SMase-2 signaling contributes both to EVs release and uptake (predominantly P4-MEV) after neonatal stroke.

Keywords

Microvesicles; Exosomes; Middle cerebral artery occlusion; Perinatal stroke; Neonate; Sphingosine-1 phosphate

1. Introduction

Neonatal arterial ischemic stroke is frequent, 1 per 2300–5000 births, and leads to long-lasting disabilities such as epilepsy, behavioral and learning deficits, and cerebral palsy (Martinez-Biarge et al., 2019). While the CNS is relatively spared from direct effects of the peripheral immune system, under physiological conditions the brain parenchyma is patrolled by perivascular macrophages and microglia while meningeal spaces are supplied with a diverse immune repertoire (Norris and Kipnis, 2019). In the early postnatal period the inflammatory response is a major brain injury component modulated both by peripheral cells and by resident immune cells in the brain—microglial cells. During physiologic brain development microglia provide local surveillance, including patrolling baseline neuronal activity (Norris and Kipnis, 2019), and can rapidly engulf overproduced neural progenitors, synaptic material and myelin sheaths (Hughes and Appel, 2020; Norris and Kipnis, 2019). Microglia can phagocytose cellular debris following neonatal injury (Fernandez-Lopez et al., 2016; Woo et al., 2012). Data have emerged that the microglial transcriptional profile, surface markers and baseline activity change during brain maturation (Keren-Shaul et al., 2017; Mrdjen et al., 2018; Tay et al., 2017b), that microglia are distinct in many ways in the brain and spinal cord (Norris and Kipnis, 2019) and are distinct from monocytes and monocyte-derived macrophages as well (Butovsky et al., 2014).

Extracellular Vesicles (EVs) as means of information exchange between cells, local or distant, is under intense investigation. It has become apparent that each single cell in the body releases EVs and that EVs are an essential part of physiological homeostasis (Stahl and Raposo, 2019), but that EVs contribute to mechanisms of diseases such as cancer, neurodegeneration and immune diseases (Karasu et al., 2018). Release of EVs is cell-type specific, the EVs “cargo” differs under both physiological conditions and after injury (Couch et al., 2017; Paolicelli et al., 2019), and age (ageing) is an important biological variable in cell-type specific EVs release (Panagiotou et al., 2018). EVs consist of exosomes (Exo) and microvesicles that are distinct not only in size, but also by the route of release from a cell and molecules they carry. Importantly, EVs contribute to brain homeostasis and neuron-glial interaction (Datta Chaudhuri et al., 2020; Delpech et al., 2019; Rajendran et al., 2014). EVs from peripheral cells can cross the brain blood barrier (BBB) and reach astrocytes, neurons and microglia (Paolicelli et al., 2019), whereas EVs produced by brains cells, neurons, for example (Pulliam et al., 2019), are found in the blood in diseases. Lipid signaling, sphinogomyelin metabolism in particular, regulate EVs biogenesis and release. Enzyme

family of sphingomyelinases (SMase)s, which are also known as SM phosphodiesterases (SMPD)s, hydrolyses sphinogomyelin and facilitates EVs biogenesis. Several studies have shown that Neutral SMase 2 (N-SMase2) plays a major role in Exo biogenesis in myeloid and other cells (Asai et al., 2015; Trajkovic et al., 2008; Xu et al., 2016b) whereas Acidic SMase 2 (A-SMase2) is proposed to mediate biogenesis of microvesicles (F. Colombo et al., 2018).

Microglia have been shown to contribute to cell-cell communication in the brain using several mechanisms, most recently by release of EVs. Microglia-derived EVs (MEV) are comprised of microvesicles (M-MEV) and Exo (M-Exo; also referred as small EVs) (Paolicelli et al., 2019; Song et al., 2019; Tay et al., 2017b). Role of MEV in biological functions was demonstrated in vitro (Murgoci et al., 2020) and microglial cells were shown to be the predominant brain cell type that take up small EVs isolated from mice following LPS administration and administered intravenously (J. J. Li et al., 2018).

Considering that microglia cells limit acute injury in a model of neonatal arterial focal stroke (Faustino et al., 2011), we asked if MEV released in ischemic-reperfused regions are the modulatory mechanism in neonatal stroke. To test this hypothesis, and to further dissect out the relative contribution of M-MEV and M-Exo, we characterized these two EVs subpopulations isolated from microglial cells that we pulled-down from acutely injured neonatal brain and maintained in culture for 4 days. We further examined uptake of MEV subpopulations by microglia from injured/matching contralateral regions in mice with disrupted signaling of N-SMase2 and show that both MEV release and uptake are suppressed in mice with disrupted N-SMase2 activity in the cortex.

2. Methods

2.1. Animals

All research conducted on animals was approved by the University of California San Francisco Institutional Animal Care and Use Committee and in accordance to the Guide for the Care and Use of Laboratory Animals (U.S. Department of Health and Human Services). Animals were given ad libitum access to food and water, housed with nesting material and shelters, and kept in rooms with temperature control and light/dark cycles. The data are in compliance with the ARRIVE guidelines (Animal Research: Reporting in Vivo Experiments). Block litter design and randomization within individual litters were used. Blinded data analysis was used where possible.

2.2. tMCAO in neonatal mice

Transient 3 h MCAO was performed using the Derugin model in postnatal day 9 (P9)-P10 C57BL/6 wild type (WT; purchased from Charles River) of both genders, as we previously described (Fernandez-Lopez et al., 2016; Woo et al., 2012). Briefly, a midline cervical incision was made under isoflurane anesthesia, the common carotid artery and internal carotid artery (ICA) exposed, single threads from a 7–0 silk suture used to temporary tie a knot below the origin of the ICA to prevent retrograde bleeding from the arteriotomy. A

coated 7–0 nylon suture was advanced 4–5 mm and removed 3 h later. Temperature was maintained.

2.3. MACS-based microglial isolation from ischemic-reperfused neonatal brain

Twenty-four hours after tMCAO, pups were perfused with ice-cold Ca^{2+}/Mg^{2+} free Hanks' BSS, brains were removed, meninges stripped, and microglial cells isolated from injured and matching contralateral regions using Neural Tissue Dissociation Kit P (Miltenyi Biotec), as we previously reported (F. Li et al., 2015). Briefly, tissue was enzymatically digested at 37 °C according the supplier protocol, myelin removed using myelin-coated magnetic beads, myelin-free cell fraction centrifuged, resuspended in 10 μl CD11b beads/90 μl degassed buffer and incubated at 4 °C for 15 min. Cells bound to $CD11b^+$-coated magnetic beads were separated using MS column (Miltenyi Biotec), counted and plated in glass 8-chamber slides for a total of 96 h, first in FBS-DMEM High glucose medium F12 for 24 h, followed by change of medium to exosome-free FBS-DMEM High glucose medium-F12 for 72 h prior to addition of labeled MEVs. We confirmed purity of isolated $CD11b^+$-microglial cells by immunostaning with Iba1, NeuN and GFAP; there were no detectible $NeuN^+$ cells, and $GFAP^+$ cells constituted <1% at 4 days after plating.

2.4. Fractionation of individual MEV populations from plated microglia isolated from injured neonatal brain

Supernatants from plated microglia isolated from injured and matching contralateral cortical regions were collected and subjected to several centrifugation steps, including 300 *g* × 10 min and then 1200 g × 10 min to remove cells and cell debris, respectively, followed by 12,000 g × 45 min to obtain Pellet 3 (P3-MEV), fraction enriched in M-MEV and, likely, large-size M-Exo. Then two-step ultra-centrifugation was used to obtain Pellet 4 (P4-MEV) (100,000 g × 2 h) and Pellet 5 (P5_MEV) M-Exo populations (200,000 g × 2 h) using Beckman Optima TL 100 Ultracentrifuge with TLA 100.3 rotor. The pellets were resuspended in 500 μl dPBS. Supernatants 3 (S3) and S5 were collected for characterization of protein markers.

2.5. Size characterization of P3-MEV and P4-MEV

To characterize size distribution, freshly collected P3-MEV and P4-MEV were analyzed by NanoSight NS300 (Malvern Instruments, UK). Samples were maintained on ice, mixed well before the analysis and vesicle sizes recorded using constant acquisition parameters applied to all experiments.

2.6. Western blot analysis in whole cortical lysates and in individual MEV fractions

P3-MEV, P4-MEV and P5-MEV pellets were resuspended in 200 μl 1X lysis buffer (Cell Signaling Technology) diluted in dPBS supplemented with protease inhibitor cocktail (Roche®, 1 mM EDTA). Whole cortical lysates from contralateral and injured cortical regions were obtained from mice perfused intracardially with 5 ml of cold PBS followed by rapid tissue dissection and snap-freezing. Tissue was homogenized in same buffer and protein concentration determined. Proteins were separated on 4–12% SDS-polyacrylamide gels (Invitrogen Life Technologies). The membranes were blocked for 1 h in 5% nonfat

dry milk or 5% BSA in TBST (20 mMTris-HCl, pH 7.6, 137 mM NaCl, 0.1% Tween 20), incubated overnight at 4 °C with the primary antibody (Table 1, Supplementary materials), and subsequently with the appropriate secondary antibodies (1 h, rt) following washes in TBST.

2.7. P3-MEV or P4-MEV uptake by microglial cells isolated from injured and uninjured brain regions

P3-MEV and P4-MEV were fluorescently labeled using mini-claret PKH Lipophilic Membrane Dye (CellVue® Claret Far Red Fluorescent Cell Linker Mini Kit for General Membrane Labeling) by resuspending pellets in 0.5 ml Diluent C, 0.5 ml exosome-free media and 3 μl CellVue® Claret (5 min, r.t.), followed by quenching with 1 ml 10%BSA in dPBS, and 1 ml of serum-free media. 700 μl of cold sucrose (0.971 M) was slowly added to the bottom of ultracentrifuge tube, MEV applied to the top, ultracentrifuged (190,000 ×g, 2 h, 4 °C), sucrose carefully aspirated and MEV^{Claret}® were resuspended in warm exosome-free media.

MEV^{Claret}® were added for 10, 30 or 120 min to plated microglia obtained from contralateral or injured regions. At each time point, cells were washed twice in warm Exo-free medium, fixed in 4% PFA and immuno-stained with Iba-1 to visualize microglia and flotillin-1 to visualize lipid rafts (BD Biosciences). Nuclei were visualized by DAPI. Images were acquired using Volocity® software 6.3.0 (Improvision/Perkin Elmer), Hamamatsu camera C4742–80-12AG (Hamamatsu Photonic Systems®), Zeiss microscope (Zeiss Axio Imager Z2) and 25× Oil objective (21 z-slices at 0.2 μm step intervals). Image analysis was performed using custom-made protocols developed in the laboratory.

2.8. Histology and immunohistochemistry

Pups were perfused intracardially with 5 ml PBS followed by 5 ml 4% PFA, brains post fixed for 24 h in 4% PFA, cryoprotected for 48 h in 30% sucrose/PBS solution, frozen and stored at −80 °C. Brains were cut coronally with cryostat (12 μm thick, spaced by 348 μm), mounted on superfrost^{+} slides and stored at −80 °C. Brain sections were blocked (5% goat serum/BSA in 1% Triton X-100, 0.1 M PBS, r.t., 1 h) and incubated overnight at 4 °C using primary antibodies described in Table 1, Supplementary materials) followed by washes and incubation with appropriate fluorescence-conjugated secondary antibodies (ThermoFisher). Slides were co-stained with Iba1 and DAPI. Microglia were isolated from injured and matching contralateral regions and plated for 4 days were stained by Iba1, flotillin-1 and DAPI. Images were captured using Zeiss microscope (Zeiss Axio imager Z2).

2.9. N-SMase2 activity

Tissue from injured and matching contralateral cortex of PBS-perfused mice was homogenized in 300 μl lysis buffer (Cell Signaling Technology) supplemented with protease inhibitor cocktail (Roche) and enzymatic N-SMase2 activity was determined in homogenates using colorometric N-SMase2 activity kit (Biovision assay kit #K192–100) based on manufacturer recommendations. OD (570 nm) was measured over a 30-min period at 37 °C. N-SMase2 activity was expressed as B/(ΔT X Q) = nmol/min/ml = mU/ml; where

B=SMase amount from the Standard Curve (nmol); ΔT = reaction time (min); Q = protein (mg). Choline standard solution and SMase substrate were generated using standard curve.

2.10. Intra-cortical injection of Smpd3 CRISPR in P7 mice

To disrupt N-SMase2 we downregulated *Smpd3* gene in the brain via intra-cortical injection of CRISPR-Cas9/Homology directed repair (HDR) plasmid. First, we standardized injection protocol by visualizing the distribution of fluorescence signal in coronally sectioned brains following bilateral intra-cortical injection of 1ul Red CellTracker™ CM-Dil (ThermoFisher) into the cerebral cortex of P7 mice (1 mm from the Bregma and 1 mm from the sagittal suture).

The CRISPR mix solution containing 0.3 μg N-SMase2 CRISPR-Cas9-KO plasmid (sc-425544, Santa Cruz Biotechnology) or Control CRISPR-Cas9 plasmid (sc-41892, Santa Cruz Biotechnology) as a negative control, was diluted 1:1 in transfection reagent (sc-395739, Santa Cruz Biotechnology) containing N-SMase2 HDR Plasmid (sc-425544-HDR, Santa Cruz Biotechnology) just before intra-cortical injection. 1 μl CRISPR-Cas9-HDR or CRISPR-Cas9/KO- HDR plasmid per left and right cortex was injected over 1 min using dispenser (PB600–1, Hamilton Company Inc.) at the coordinates defined above.

2.11. Statistical analysis

Block litter design was used in mice of both sexes and analysis performed in blinded manner. GraphPad Prism 8 software (GraphPad) was utilized for statistical analysis. Several types of analyses were used depending on the parametric/non-parametric data distribution and the number of groups compared, as listed individual figure legends. Unpaired *t*-test was used in Fig. 1F, Mann-Whitney *U* test used in Figs. 1A, 4A and 6E. Two-way ANOVA was used to compare multiple groups with independent variables followed by Tukey's multiple comparisons test (differences between ipsilateral and contralateral regions and either over time or for respective differences in contralateral or ipsilateral regions of Smpd3/Ct and Smpd3/KD; (Figs. 2D, F, 3B, H, I, 4D, F, 5B–E, 6A, 6D). Each dot on all graphs represents individual measurement. Individual *p* values are listed in figures for data that are significant. Results are shown as mean ± SD.

3. Results

3.1. Characterization of microglia isolated from neonatal brain 24 h after ischemia-reperfusion

First, we characterized microglial cells isolated using CD1lb-conjugated magnetic beads from naïve P10 brain and from injured and matching contralateral cortical regions 24 h after tMCAO in P9-P10 pups. The number of microglial cells pulled down from injured cortex was significantly higher compared to that in naïve mice or contralateral regions of mice subjected to tMCAO ($p = 0.0021$ and $p = 0.0126$, respectively; Fig. 1A), consistent with our previous report (F. Li et al., 2015). At 4 days in culture, the number of $Iba1^+$ cells and the overall $Iba1^+$ coverage of plated cells were similar after plating cells at the same density (Fig. 1B and C). Morphology of cells derived from contralateral or ipsilateral cortex

was diverse, with some cells exhibiting multiple long processes (arrow) while some cells exhibitted shortened processes (arrowhead; Fig. 1D).

3.2. Characterization of MEV subpopulations

Next we characterized MEV from naïve and injured neonatal brain. Considering that the number of EVs markers keeps growing and concepts for which of them are unique to each of the two EVs subpopulations, microvesicles and Exo, continue to evolve (Xu et al., 2016a) and that age, time after injury and MEV isolation method can affect the cargo (Karasu et al., 2018; Nakai et al., 2016; Xu et al., 2016a), we established multi-step centrifugation protocol in conjunction with multi-marker characterization of MEV populations. MEV fractions included P3-MEV, pellet following 12,000 ×*g* centrifugation that contains microvesicles and, likely, large size M-Exo, and P4-MEV, pellet following 100,000 ×*g* centrifugation that contains M-Exo; and P5-MEV, pellet following 200,000 ×*g* centrifugation that contains M-Exo. We also collected S3 and S5 supernatants for characterization of individual markers in individual centrifugates.

Analysis of EVs size distribution by Nanosight showed significantly different average size for P3-MEV and P4-MEV, as evident from images (Fig. 1E right) and graphs depicting size distribution (Fig. 1E left). P3-MEV average size was 135.42 ± 75.22 nm and 116.00 ± 51.50 nm for P4-MEV (Fig.1F).

The pattern of expression of proteins involved in the biogenesis of EVs in P3-MEV, P4-MEV and P5-MEV fractions was molecule-specific. P4-MEV and P5-MEV, and not P3-MEV, were enriched in Rab5, GTPase involved in early endosome vesicular trafficking, whereas P3-MEV was enriched in Rab11, GTPase involved in late endosome trafficking and transport of endolysosomal vesicles toward the plasma membrane (Fig. 1G). P4-MEV fraction was enriched in LAMP2. P4-MEV and P5-MEV were enriched in S1P, a substrate for S1PRs and a modulator of cell homeostasis (Fig. 1G). P4-MEV and P5-MEV were enriched in EHD4 and HSP20, proteins frequently used as exosome markers (Fig. 1G). It is known that EVs from various cell types can carry various inducible molecules. Examination of ICAM-1 expression showed its enrichment in P4-MEV and P5-MEV, particularly in MEV from injured brain regions (Fig. 1G). None of these proteins were observed in PBS buffer used as negative control (Fig. 1G).

Together, these results demonstrate that P3-MEV and P4-MEV are different in their size and composition of markers of vesicular trafficking related to EVs biogenesis and release. Furthermore, P4-MEV predominantly carried ICAM-1, protein known to mediate endothelial activation in stroke.

3.3. Uptake of MEV by cultured microglia pulled down from injured and contralateral cortical regions 24 h after tMCAO

We then examined whether two MEV subpopulations interact with microglial cells. Incubation of plated microglial cells with P3-MEV or P4-MEV collected from cells isolated from contralateral or injured cortex did not alter total cell coverage or the number of adherent cells per field-of-view (FOV, Fig. 2A and B). Within the cells, P3-MEV$^{Claret®}$ and P4-MEV$^{Claret®}$ accumulated in the cytoplasm and in organelles, and only some were

observed in the cellular processes (Fig. 2C). Previous reports suggested accumulation of microvesicles, not Exo, in lipid raft-associated scaffolding domains rich in flotillin-1. We observed that larger size P3-MEV$^{Claret®}$ colocalized with flotillin (Fig. 2C).

Next, we quantified uptake of fluorescently labeled MEV originated from injured (P3-MEV$^{Claret®\text{-}Ipsi}$) or contralateral (P3-MEV$^{Claret®\text{-}Contra}$) cortex by microglial cells from injured ($^{Ipsi\text{-}}$microglia) or contralateral ($^{Contra\text{-}}$microglia) cortex. Uptake of P3-MEV$^{Claret®\text{-}Ipsi}$ by $^{Ipsi\text{-}}$microglia was significantly higher compared to uptake of P3-MEV$^{Claret®\text{-}Contra}$ by $^{Contra\text{-}}$microglia at all three time points studied, after 10, 30 and 120 min of incubation ($p < 0.0001$, $p = 0.0055$, and $p = 0.0446$, respectively; Fig. 2D). Uptake of P3-MEV$^{Claret®\text{-}Ipsi}$ by $^{Ipsi\text{-}}$microglia was significantly decreased between 10 min and 120 min ($p = 0.0096$, Fig. 2D). Uptake of P3-MEV$^{Claret®\text{-}Contra}$ by $^{Ipsi\text{-}}$microglia remained low, at levels observed for $^{Contra\text{-}}$microglia (Fig. 2E).

Uptake of P4-MEV$^{Claret®\text{-}Ipsi}$ and P4-MEV$^{Claret®\text{-}Contra}$ from same mice examined in parallel showed an overall similar pattern, i.e., significantly increased uptake of P4-MEV$^{Claret®\text{-}Ipsi}$ by $^{Ipsi\text{-}}$microglia (Fig. 2F). Uptake was the highest 10 min after incubation ($p < 0.0001$) and lower but significant at 30 min ($p = 0.0359$, Fig.2F). Uptake of P4-MEV$^{Claret®\text{-}Ipsi}$ by $^{Ipsi\text{-}}$microglia was significantly decreased from 10 min to 30 and 120 min ($p < 0.0001$, Fig. 2F). P4-MEV$^{Claret®\text{-}Contra}$ uptake by $^{Ipsi\text{-}}$microglia remained at the basal levels (Fig. 2G). The magnitude of P3-MEV and P4-MEV uptake was within the same range.

Together these data establish that the source of P3-MEV and P4-MEV—microglia activated by ischemia-reperfusion or basal state microglia—affects their recognition and uptake and that activation status of microglial cells also determines the magnitude of uptake.

3.4. The pattern of N-SMase2 expression and activity is altered by neonatal stroke

N-SMase2 was shown to mediate EVs release from cells (Verderio et al., 2018). To understand the role of N-SMase2 and N-SMase2-dependent MEV function in neonatal stroke, we examined N-SMase2 enzymatic activity in naïve and injured pups. N-SMase2 activity increased significantly from P10 to P12 and from P11 to P12 ($p = 0.0016$ and $p = 0.0343$, respectively) in naïve pups (Fig. 3A). tMCAO rapidly and markedly decreased N-SMase2 activity in injured cortex by 3 h after reperfusion ($p = 0.0252$, Fig. 3B) and produced bilateral decrease of N-SMase2 activity at 13 h after reperfusion ($p = 0.0002$, Fig. 3B). While activity was increased in contralateral regions by 72 h after reperfusion compared to that at 3 and 13 h ($p < 0.0001$), it remained significantly lower in injured cortex ($p < 0.0001$, Fig. 3B), but higher than at 3 h ($p = 0.0183$) and 13 h after reperfusion ($p < 0.0001$, Fig. 3B).

N-SMase2 was abundantly expressed in NeuN^{+} neurons in naïve mice (Fig. 3C), in contralateral cortex (not shown) and outside of injured region in morphologically intact neurons (Fig. 3D–F, arrowheads), whereas N-SMase2 expression was lost in injured neurons in ischemic-reperfused regions (Fig.3D, on the right from punctate line). At the same time, in injured regions, N-SMase2 expression was increased in CD68^{+} microglia/macrophages (Fig. 3D and E, arrows). Few morphologically intact neurons within injured region

expressed N-SMase2 (Fig. 3E, arrowheads). We did not observe N-SMase2 in reactive GFAP$^+$ astrocytes localized outside of lesioned regions (Fig. 3F).

Together these data demonstrate that the patterns of N-SMase2 expression are cell-type specific in the neonatal brain, with neurons as predominant cell source of expression under physiological conditions and N-SMase2 upregulation after tMCAO in activated microglia/macrophages, in parallel to loss in expression in injured and dying neurons.

3.5. Diminished N-SMase2 activity protects neonatal brain but does not affect vascular coverage or accumulation of microglia/macrophages in injured region

Next we asked if inactivation of N-SMase2 affects injury after neonatal stroke. Using gene editing tool, CRISPR-Cas9, coupled with HDR strategy, we downregulated the gene that codes for N-SMase2, Smpd3, 2 days before tMCAO. In pilot tests we developed a protocol for intra-cortical vector injection using CellTracker™ CM-DiI (data not shown). We then confirmed CRISPR-Cas9 expression by the presence of N-Smase2/HDR (fluorescence in proximity to injection) 3 and 5 days after administration (Red, Fig. 3G).

In naive brain, intracortical injection of a CRISPR-Cas9/KO-HDR for Smpd3 (Smpd3/KD) at P7 led to gradual decrease of N-SMase2 activity overtime, with a trend in decrease at P10 (ns) and significant reduction at P12 ($p = 0.0041$, Fig. 3H). N-SMase2 activity remained unchanged in pups from same litters treated with plasmid control CRISPR-Cas9/Ct-HDR (Smpd3/Ct) (Fig. 3A compared Fig. 3H).

At 72 h after tMCAO, N-SMase2 activity was significantly reduced in injured cortex of Smpd3/Ct mice ($p < 0.0001$, Fig. 3I), similar to that in injured regions of non-treated mice (Fig. 3B) and compared to that in respective contralateral regions ($p = 0.0069$, Fig. 3I). N-Smase2 was significantly decreased in contralateral cortex by Smpd3/KD administration ($p = 0.0031$, Fig.3I).

Examination of HDR presence in pups treated with Smpd3/Ct or Smpd3/KD and subjected to tMCAO showed HDR expression in injured regions in both groups. In Smpd3/KD-treated pups HDR was observed in most of CD68$^+$ or IB4$^+$ activated microglia/macrophages at 24 h after tMCAO (Fig. 3J) and in injured and peri-lesioned regions 72 h after tMCAO (Fig. 3K, white arrowheads) but in some CD68$^+$ or IB4$^+$ cells expression was either low (thin white arrows) or not evident (white asterisk). HDR expression was high in few cells CD68$^-$ cells (Fig. 3J). In peri-lesioned regions a number of CD68$^-$ cells with neuron-like morphology did not express HDR expressed N-SMase2 (Fig. 3K), whereas HDR$^+$ cells showed low-to-none N-SMase2 expression (Fig. 3K, yellow asterisk).

Histological examination 72 h after tMCAO showed injury volume in Smpd3/Ct treated mice similar to our historic injury volume in non-treated mice (Chip et al., 2017). Injury volume was significantly smaller in Smpd3/KD than in Smpd3/Ct mice ($p = 0.0043$, Fig. 4A–B). tMCAO similarly decreased coverage of Glut1$^+$-vessels in injured regions of Smpd3/Ct and Smpd3/KD mice ($p = 0.0315$ and $p = 0.0204$ respectively, Fig. 4C–D). tMCAO also led to significantly increased number of Iba1$^+$-microglia/macrophages in ischemic-reperfused regions in both groups (Smpd3/Ct, $p < 0.0001$ and Smpd3/KD, $p =$

0.0085); there were no significant differences between groups due to the treatment (Fig. 4D, F). These data show that decreased N-Smase2 activity in the cortex offers beneficial effect against injury without effects on vascular coverage or morphological transformation/activation of microglia.

3.6. Effects of Smpd3 gene downregulation on MEV uptake by microglial cells from naïve and injured neonatal brain

Downregulation of *Smpd3* in the brain did not change morphology of isolated and plated microglia incubated with P3-MEV (Fig. 5A) or P4-MEV (not shown). Based on total protein per 10^6 plated microglial cells isolated from contralateral and ipsilateral regions, P3-MEV yield was similar in non-treated, Smpd3/Ct and Smpd3/KD pups (not shown). P4-MEV^{Contra} and P4-MEV^{Ipsi} yields were similar in non-treated mice. A tendency toward increased yield of P4-MEV^{Ipsi} compared to P4-MEV-^{Contra} was observed in Smpd3/Ct mice (2.4 ± 0.8 Vs. 4.80 ± 1.87 mg/10^6 cells, respectively; $n = 3$ per group, $p = 0.095$) but increase in P4-MEV^{Ipsi} was abolished in Smpd3/KD (2.58 ± 1.08 Vs. 2.92 ± 1.32 mg/10^6 cells, n = 3 per group; ns), suggesting that N-SMase2 disruption adversely affects the magnitude of P4-MEV release from activated microglia obtained from injured regions.

We then determined how downregulation of *Smpd3* in the cortex of neonatal mice affects MEV uptake by microglia from acutely injured brain. Basal uptake level of P3-MEV$^{Claret®-Contra}$ from untreated mice (i.e., by microglia from contralateral region) and from Smpd3/Ct mice were similar, 6.33 ± 2.79 Vs. 5.26 ± 3.62 P3-MEV per Iba1$^+$ cell, respectively (Supplementary Fig. 1A). Uptake of P3-MEV$^{Claret®-Contra}$ from Smpd3/Ct by $^{Ipsi-}$microglia from both Smpd3/Ct and Smpd3/KD mice was significantly increased compared to uptake by $^{Contra-}$microglia from respective Smpd3/Ct and Smpd3/KD mice ($p < 0.0001$ and $p = 0.0456$ respectively, Fig. 5B). There was a significant but lower uptake increase by $^{Ipsi-}$microglia from Smpd3/KD mice than from Smpd3/Ct mice ($p = 0.0393$). Uptake of P3-MEV$^{Claret®-Ipsi}$ from Smpd3/Ct-^{Ipsi} was also significantly increased by microglia from injured region of Smpd3/Ct mice ($p < 0.0001$, Fig. 5C). However, no increase in uptake occurred by microglia from Smpd3/KD mice. Significantly lower uptake by $^{Ipsi-}$microglia from Smpd3/KD mice ($p = 0.0019$, Fig. 5C) suggested a role for N-SMase2 for MEV recognition/uptake by microglial cells.

Uptake of P3-MEV$^{Claret®-Contra}$ from Smpd3/KD mice by $^{Ipsi-}$microglia from Smpd3/Ct was significantly increased compared to $^{Contra-}$microglia in same mice ($p < 0.0001$), whereas uptake by $^{Ipsi-}$microglia from Smpd3/KD was abolished ($p < 0.0001$, Fig. 5D). Significantly increased uptake of P3-MEV$^{Claret®-Ipsi}$ from Smpd3/KD by $^{Ipsi-}$microglia from Smpd3/Ct was observed ($p < 0.0001$), compared to $^{Contra-}$microglia from respective mice but uptake was abolished in $^{Ipsi-}$microglia from Smpd3/KD ($p < 0.0001$, Fig. 5E). Together, these data demonstrate that N-SMase2 inhibition in the neonatal brain reduces both the release and uptake of P3-MEV by activated microglia with inhibited N-SMase2. Consistent with functional outcomes (release and uptake), immunolabeling of plated microglial cells with HDR and N-SMase2 showed continued presence of HDR label even after 4 days after plating microglia from injured Smpd3/Ct and Smpd3/KD pups (Fig. 5F) as well as reduced N-SMase2 expression in HDR$^+$ cells from Smpd3/KD pups compared to that

in Smpd3/Ct pups (Fig. 5F). Reduced N-SMase2 expression in microglia from injured regions of Smpd3/KD pups compared to that in injured regions of Smpd3/Ct pups was also confirmed by Western blot (Fig. 5G).

We then examined whether disruption of N-SMase2 activity affects the ability of microglial cells to recognize and uptake P4-MEV isolated from same microglia (Fig. 6). P4-MEV$^{Claret®\text{-}Contra}$ uptake by ^{Contra}-microglia from untreated and Smpd3/Ct mice were similar, 7.07 ± 3.06 Vs. 5.90 ± 3.89 P3-MEV per Iba1^{+} cell, respectively (Suppl. Fig. 1B). P4-MEV$^{Claret®\text{-}Contra}$ uptake from Smpd3/Ct was significantly increased by ^{Ipsi}-microglia from Smpd3/Ct ($p = 0.0021$) but was completely abolished in ^{Ipsi}-microglia from Smpd3/KD mice ($p = 0.0026$, Fig. 6A). The same pattern was observed for P4-MEV$^{Claret®\text{-}Ipsi}$ increased uptake by ^{Ipsi}-microglia from Smpd3/Ct ($p = 0.0070$) but unchanged uptake by ^{Ipsi}-microglia from Smpd3/KD mice ($p < 0.0001$, Fig. 6B). A much smaller but significant increase in uptake of P4-MEV$^{Claret®\text{-}Contra}$ from Smpd3/KD mice was observed by ^{Ipsi}-microglia from Smpd3/Ct and Smpd3/KD mice ($p = 0.0399$ and $p = 0.0023$ respectively, Fig. 6C), but uptake of P4-MEV$^{Claret®\text{-}Ipsi}$ from Smpd3/KD mice by $^{Contra/Ipsi}$-microglia of Smpd3/Ct and Smpd3/KD mice remained at basal levels (Fig. 6D).

Comparisons of P3-MEV and P4-MEV uptake showed selective suppression of P4-MEV$^{Claret®\text{-}Contra}$ uptake by microglia from Smpd3/KD mice ($p = 0.0211$, Fig. 6E). Therefore, diminishing N-SMase2 activity predominantly reduces recognition of P4-MEV. Together these data show that inhibition of N-SMase2 in the brain affects vesicle recognition.

4. Discussion

The role of MEV as the modulatory mechanism of neonatal stroke has never been explored. We demonstrate for the first time that in healthy neonatal brain microglial cells release both microvesicles and Exo, that these EVs subtypes have distinct morphological and “cargo” characteristics, and that uptake of both MEV subtypes by activated microglia derived from ischemic-reperfused regions is significantly higher than by microglia from contralateral region. We show that disruption of N-SMase2 signaling before stroke via downregulation of *Smpd3* gene in the brain (using CRISPR-dCas9 methodology) attenuates injury, in part via altered lipid metabolism and EVs biogenesis in neurons and in activated microglia. We then show that interrupted N-SMase2 function in vivo not only reduces vesicular release from microglia derived from ischemic-reperfused neonatal brain but significantly diminishes MEV recognition and uptake by activated microglia, particularly M-Exo.

Microglia are central to the crosstalk between cells in the brain (Tay et al., 2017a) and between periphery and the brain, signaling in part via EVs (Balusu et al., 2016; Panagiotou et al., 2018). Historically, microglia were viewed as contributors to stroke injury by producing inflammatory mediators (Vexler and Yenari, 2009). However, as endogenous brain macrophages, microglia remove dying neurons by phagocytosis and are a major source of growth factors (Ueno et al., 2013). Microglial malfunction makes the developing brain prone to infection (Dinel et al., 2016) and, as we previously demonstrated using pharmacological strategies to deplete microglia or eliminate individual signaling

mechanisms in these cells, microglia protect against acute neonatal stroke (Fernandez-Lopez et al., 2016; Woo et al., 2012). Here we examined whether microglia are a major source of MEV in the immature brain and how neonatal stroke affects microglia-MEV interaction.

Literature has emerged on EVs as an important mechanism of cell-to-cell signaling under physiological and disease conditions, that essentially all cells in the body release EVs, with cell-type specific properties of EVs and their "cargo", and that both EVs types—microvesicles (also called ectosomes) and Exo—contribute to transfering biomolecules among cells and influencing the extracellular microenvironment. It is also recognized that biogenesis and release mechanisms are EVs subtype specific; microvesicles are generated at the plasma membrane whereas Exo are formed inside multivesicular bodies (MVBs) through two membrane inversion processes, forming intraluminal vesicles and then fusion of MVBs with the plasma membrane. Both EVs subtypes were shown to contain diverse groups of molecules but EVs themselves and their protein, DNA and coding and non-coding RNA "cargo", which are markedly different in healthy and diseased organisms (E. Colombo et al., 2012; Debayon and Pachter, 2015; Gupta and Pulliam, 2014; Gyorgy et al., 2015; Kanada et al., 2015; Lai and Breakefield, 2012; Paolicelli et al., 2019; Pérez-Boza et al., 2018; Rajendran et al., 2014; Testai et al., 2012; Verderio et al., 2012).

EVs, M-MEV in particular, first gained attention as a major mechanism of intercellular communication in neurodegenration when M-MEV accumulation in the CSF of multiple sclerosis patients and in rat experimental allergic encephalomyelitis (EAE) model was shown to promote the disease by carrying inflammatory mediators (Verderio et al., 2012), IL-1β release in particular (Bianco et al., 2009). Release of M-MEV was more efficient from activated than from resting microglia (Bianco et al., 2009) and ATP, which is released from damaged cells and serves as a danger signal and chemoattractant for microglia, triggered M-MEV release (Verderio and Matteoli, 2001). EVs were shown to modulate stroke and brain trauma outcomes (Hazelton et al., 2018; Xin et al., 2014) and BBB integrity (Paul et al., 2016) in the adult. M-Exo were shown as tau carriers in the in vitro and in vivo experiments following microglial deletion or inhibition of exosome synthesis (Asai et al., 2015). At the same time, EVs serve as mediators of synaptic activity (Bianco et al., 2009) and promote immune homeostasis in activated and aged microglia (Udeochu et al., 2018). In vitro studies of immortalized BV2 showed beneficial role of MEV after exposure to various toxic stimuli, in part by transporting factors involved in cell survival.

To understand how tMCAO in neonatal mice affects communication of MEV with homeostatic and activated microglia and begin gaining knowledge of potential therapeutic effects of M-MEV and M-Exo, we pulled down microglial cells from injured and matching contralateral cortex immuno-magnetically using $CD11^{+}$-conjugated magnetic beads at 24 h after reperfusion, a time point post-reperfusion that we chose based on our observations that the number of infiltrated $CD11^{+}/CD45^{high}$ monocytes/macrophages (Chip et al., 2017) and $CCR2^{RFP/+}$ monocytes/macrophages (Fernandez-Lopez et al., 2016) are low in injured regions of the neonatal brain. Consistent with our previous report that microglia isolated from ischemic-reperfused neonatal brain retain "memory" of their activation in vivo, as was manifested by increased number of pulled-down $CD11^{+}$-cells resultant from proliferation and migration and increased expression of inflammatory mediators after plating microglia

(TLRs expression, (F. Li et al., 2015)), in this study the number of pulled-down microglia was increased compared to that in contralateral cortex. We further ascertained that upon plating microglial population derived from injured and uninjured regions is free of neurons, endothelial cells and other glial cells. Finally, considering that M-MEV and M-Exo have distinct structural-functional "signatures" (Kanada et al., 2015) and can carry non-overlapping "cargo" (Lawson et al., 2017; Paolicelli et al., 2019; Verderio et al., 2018) and, as such, mediate distinct biological effects in the brain, we used multi-step centrifugation protocol to isolate P3-MEV and P4-MEV and P5-MEV, assuming that P3-MEV contain both microvesicles and large M-Exo, while pellets from ultracentrifugation contain M-Exo only.

Nanoparticle tracking analysis showed a range of vesicle size, with most abundant P4-MEV size around 100 nm and P3-MEV size around 145 nm. Our step-wise centrifugation protocol and multiple peaks in size observed in P3-MEV population suggested that the latter fraction predominantly consists of M-MEV, but that M-Exo contribute as well. By Western Blot analysis we then confirmed the presence of cell type-specific factor Iba-1 in all MEV fractions and identified distinct protein "cargo" carried by P3-MEV and P4-MEV. Microvesicles and Exo were previously thought to have unique markers but vast majority of identified Exo markers (ExoCarta; http://www.exocarta.org) are shared by microvesicles as well (Lawson et al., 2017) including tetraspanins (CD9, CD63 and CD81), MVB formation proteins (Alix, Tsg101), and ESCRT proteins (endosomal sorting complex required for transport) (Henne et al., 2011). Even further, not all Exo necessarily express all tetraspanins and other commonly used markers (Greening and Simpson, 2018) and EVs isolation conditions can greatly affect purity of EVs population (Xu et al., 2016a), "cargo" and size distribution (Karasu et al., 2018; Nakai et al., 2016). For these reasons rather than centering on tetraspanins, we focused on characterizing proteins involved in biogenesis, including proteins associated with endocytotic machinery (Rab5, Rab11, LAMP2), lipid signaling involved in EVs release (S1P), accepted markers of Exo (EHD4, Hsp20) and inducible inflammatory mediators (ICAM-1). S3 supernatant and P4-MEV (M-Exo) selectively expressed endolysosomal protein LAMP2, endocytotic GTPase Rab5 and EHD4, which localizes to Rab5/Arf6-containing endosomes and is implicated in the regulation of endocytic trafficking (Sharma et al., 2008). P4-MEV was also enriched in lipid mediator S1P. Rab11 was present in both vesicular subtypes but its expression was highly enriched in P3-MEV.

Using a combination of in vivo tMCAO model and a model of plated microglia derived from neonatal brain after acute injury (in vitro), we show that microglial cells are both the source of and recipients of M-MEV and M-Exo in neonatal brain and that MEV-microglial interactions are greatly enhanced in injured regions. In particular, we demonstrate that microglial cells uptake both P3-MEV and P4-MEV (i.e., M-MEV and M-Exo) and that uptake of MEV, unlabeled or fluorescently labeled with mini-claret PKH lipophilic membrane dye, does not change cell morphology. Immunofluorescence to examine P3-MEV and P4-MEV distribution within the cells showed both types of MEV in the cytosol, in the organelles, with some MEV seen in processes. P3-MEV colocalized with the lipid raft marker Flotillin-1. Although there was no significant difference in release of P3-MEV or P4-MEV from plated microglia obtained from injured and contralateral cortex, the state of activation in vivo at the time of isolation manifested in plated microglia by significantly

higher MEV uptake by microglia from ischemic-reperfused region compared to that by microglia in naïve or in uninjured brain regions. Uptake was rapid, with maximum at 10 min.

MEV were shown to carry inflammatory molecules in adult injury models, such as cytokines, MMPs and ICAM-1 (Gupta and Pulliam, 2014; Han et al., 2019; Karasu et al., 2018). Proteomic analysis in adult stroke showed that the EVs membrane is rich in integrin and adhesion molecules (Couch et al., 2017) and that Exo derived from immune cells contain antigen peptide/MHC complexes and various antigens (Hiltbrunner et al., 2016). We show that M-Exo and not P3-MEV are enriched in inflammatory mediator ICAM-1 and that packaged ICAM-1 concentration is higher in M-Exo from injured regions.

We then tested effects of disrupted activity of N-SMase2, an enzyme that catalyzes sphingomyelin hydrolysis and mediates EVs release and intercellular communication (Airola et al., 2017). N-SMase2 is ubiquitously expressed in the body (J. Li et al., 2016; Zhou et al., 2019), is highly expressed in neurons and astrocytes (Dinkins et al., 2014; Stoffel et al., 2018) (Dinkins et al., 2014) and is localized in Golgi compartment (Tomiuk et al., 2000) and inner leaflet plasma membrane (Tani and Hannun, 2007). N-Smase2 activity is prominent during postnatal development by modifying lipid bilayer and Golgi secretory pathway (Stoffel et al., 2005). *Smpd3*, the gene which codes for N-SMase2, is specifically involved in Exo release via MVB (Garner et al., 2020) and by microvesicular release from plasma membrane (Lawson et al., 2017). Lack of N-SMase can abort EVs function and alter neuron-microglial communication (Bianco et al., 2009; Trajkovic et al., 2008; Wacker et al., 2012). *Smpd3* deficient mice show disturbances in neuronal architecture and progressive cognitive impairment (Stoffel et al., 2016; Stoffel et al., 2018), in part by impeding remodeling of the lipid bilayer in Golgi essential for budding and formation of MVB and leading to accumulation of neurotoxic proteins in the cell (Stoffel et al., 2005). Pharmacological inhibition of N-SMase2 in BV2 microglia by GW4869 also leads to reduced M-Exo production (Udeochu et al., 2018).

We observed significant developmental increase in N-SMase2 enzymatic activity between P10 and P12 and cortical neurons as the predominant cellular source of N-SMase2 under physiological conditions. Following tMCAO, neurons in the contralateral regions and in uninjured region ipsilateral to tMCAO (the cingulate) continued express N-SMase2 whereas injured/dying neurons no longer expressed N-SMase2. Although N-SMase2 was induced in activated microglia/macrophages in injured regions, the net change in N-SMase2 activity within 72 h after tMCAO was a decrease in activity because of loss of neuronal N-SMase2 activity. Smpd3 downregulation in the brain before stroke via CRISPR/dcas9 editing gradually decreased N-SMase2 activity. Disruption of M-Exo biogenesis by inhibiting N-SMase2 reduced injury volume 72 h after tMCAO without affecting the vascular coverage. While these data suggest that reducing EVs release is neuroprotective, they do not allow us discriminate whether reduced injury is a consequence of N-SMase2 deactivation in neurons as the major cell type expressing N-SMase2 or due to reducing EVs release from activated microglia that we demonstrated. Findings that P3-MEV yield from microglia from contralateral and ipsilateral regions was similar in non-treated, Smpd3/Ct and Smpd3/KD pups but P4-MEV yield from ipsilateral regions was increased and susceptible to N-SMase2

disruption (i.e., decrease in Smpd3/KD) suggest distinctions in EVs producing machinery in microglia.

Characterization of MEV properties/function in neonatal stroke using a model of pulled-down microglia from acutely injured/uninjured neonatal brain is the first step toward improving the understanding of EVs surface ligands and EVs "cargo" potentially capable of modulating injury, but there are many unanswered questions in this first study of the role of MEV in injury. First, while we established novel effects of injury-dependent changes in MEV-microglia interactions, we did not examine the "cargo" besides enhanced inducible mediator ICAM-1 in M-Exo from injured regions. Thus, we can only speculate that other inflammatory and anti-inflammatory molecules can be carried by P3-MEV and P4-MEV. We also recognize that proteins from P4-MEV fraction could to some extent contribute to P3-MEV-mediated signaling. Second, while we focused on protein markers, RNAs as part of "cargo" have been a major focus in EVs studies in adults, with demonstrated beneficial and injurious effects. The latter direction would be especially important given that some data suggest that a single exosome can contain more than several thousand of mRNAs or miRNAs (Pérez-Boza et al., 2018) and that some miRNAs can be specific to MEV (Lemaire et al., 2019). Third, data continue to accumulate on bi-directional communication between neurons and microglia. For example, uptake of Exo produced by neurons and other glia by microglia has been previously demonstrated (Fitzner et al., 2011; Fruhbeis et al., 2013). While our data clearly demonstrate that N-SMase-2 signaling contributes both to vesicular release and uptake after neonatal stroke, further studies are needed to dissect-out precise mechanisms of N-SMase2 disruption, i.e., whether observed protection is consequent to reduced EVs release from neurons or from activated microglia. Altogether, demonstration that microglial cells are both the source of and recipients of M-MEV and M-Exo in neonatal brain and that injury enhances MEV-microglial interactions provide some cues and suggest that microglia can modify injury in neonatal stroke at least in part via MEV, warranting future studies of effects of MEV in neonatal brain injury.

Supplementary Material

Refer to Web version on PubMed Central for supplementary material.

Acknowledgements

The work was supported by NIH/NINDS RO1 HL139685 (ZV), RO1 NS44025 (ZV), RO1 NS76726 (ZV), 17IRG33430004 (ZV).

Abbreviations:

BBB	blood-brain barrier
Contra	contralateral region
CRISPR/Cas9-KO	Clustered Regularly Interspaced Short Palindromic Repeats/Cas9
EVs	extracellular vesicles

Exo	exosomes
HDR	Homology directed repair
Ipsi	injured region
MEV	microvesicles
M-MEV	microglial microvesicles
MVBs	multivesicular bodies
M-Exo	microglial exosomes
N-SMase2	neutral sphingomyelinase 2
P3-MEV	Pellet 3 of microglial microvesicles
P4-MEV	Pellet 4 of microglial microvesicles
P5-MEV	Pellet 5 of microglial microvesicles
P9	postnatal day 9
tMCAO	transient middle cerebral artery occlusion
Smpd3/KD	Smpd3 knockdown
S3	supernatant 3

References

Airola MV, Shanbhogue P, Shamseddine AA, Guja KE, Senkal CE, Maini R, Bartke N, Wu BX, Obeid LM, Garcia-Diaz M, Hannun YA, 2017. Structure of human nSMase2 reveals an interdomain allosteric activation mechanism for ceramide generation. Proc. Natl. Acad. Sci. U. S. A 114, E5549–e5558. [PubMed: 28652336]

Asai H, Ikezu S, Tsunoda S, Medalla M, Luebke J, Haydar T, Wolozin B, Butovsky O, Kügler S, Ikezu T, 2015. Depletion of microglia and inhibition of exosome synthesis halt tau propagation. Nat. Neurosci 18, 1584–1593. [PubMed: 26436904]

Balusu S, Van Wonterghem E, De Rycke R, Raemdonck K, Stremersch S, Gevaert K, Brkic M, Demeestere D, Vanhooren V, Hendrix A, Libert C, Vandenbroucke RE, 2016. Identification of a novel mechanism of blood-brain communication during peripheral inflammation via choroid plexus-derived extracellular vesicles. EMBO Mol. Med 8, 1162–1183. [PubMed: 27596437]

Bianco F, Perrotta C, Novellino L, Francolini M, Riganti L, Menna E, Saglietti L, Schuchman EH, Furlan R, Clementi E, Matteoli M, Verderio C, 2009. Acid sphingomyelinase activity triggers microparticle release from glial cells. EMBO J. 28, 1043–1054. [PubMed: 19300439]

Butovsky O, Jedrychowski MP, Moore CS, Cialic R, Lanser AJ, Gabriely G, Koeglsperger T, Dake B, Wu PM, Doykan CE, Fanek Z, Liu L, Chen Z, Rothstein JD, Ransohoff RM, Gygi SP, Antel JP, Weiner HL, 2014. Identification of a unique TGF-beta-dependent molecular and functional signature in microglia. Nat. Neurosci 17, 131–143. [PubMed: 24316888]

Chip S, Fernandez-Lopez D, Faustino J, Li F, Derugin N, Vexler ZS, 2017. Genetic deletion of galectin-3 enhances neuroinflammation, affects microglial activation and contributes to sub-chronic injury in experimental neonatal focal stroke. Brain Behav. Immun 60, 270–281. 10.1016/j.bbi.2016.11.005. Feb. (Epub 2016 Nov 9). [PubMed: 27836669]

Colombo E, Borgiani B, Verderio C, Furlan R, 2012. Microvesicles: novel biomarkers for neurological disorders. Front. Physiol 3, 63. [PubMed: 22479250]

Colombo F, Bastoni M, Nigro A, Podini P, Finardi A, Casella G, Ramesh M, Farina C, Verderio C, Furlan R, 2018. Cytokines stimulate the release of microvesicles from myeloid cells independently from the P2X7 receptor/acid sphingomyelinase pathway. Front. Immunol 9, 204. [PubMed: 29467770]

Couch Y, Akbar N, Davis S, Fischer R, Dickens AM, Neuhaus AA, Burgess AI, Rothwell PM, Buchan AM, 2017. Inflammatory stroke extracellular vesicles induce macrophage activation. Stroke 48, 2292–2296. [PubMed: 28536169]

Datta Chaudhuri A, Dasgheyb RM, DeVine LR, Bi H, Cole RN, Haughey NJ, 2020. Stimulus-dependent modifications in astrocyte-derived extracellular vesicle cargo regulate neuronal excitability. Glia 68, 128–144. [PubMed: 31469478]

Debayon P, Pachter J, 2015. Extracellular vesicles as possible conveyors of tight junction protein to leukocytes in neuroinflammation. In: International Society for Extracellular Vehicles Washington, DC.

Delpech JC, Herron S, Botros MB, Ikezu T, 2019. Neuroimmune crosstalk through extracellular vesicles in health and disease. Trends Neurosci. 42, 361–372. [PubMed: 30926143]

Dinel AL, Rey C, Baudry C, Fressange-Mazda C, Le Ruyet P, Nadjar A, Pallet P, Joffre C, Laye S, 2016. Enriched dairy fat matrix diet prevents early life lipopolysaceharide-induced spatial memory impairment at adulthood. Prostaglandins Leukot. Essent. Fat. Acids 113, 9–18.

Dinkins MB, Dasgupta S, Wang G, Zhu G, Bieberich E, 2014. Exosome reduction in vivo is associated with lower amyloid plaque load in the 5XFAD mouse model of Alzheimer's disease. Neurobiol. Aging 35, 1792–1800. [PubMed: 24650793]

Faustino J, Wang X, Jonhson C, Klibanov A, Derugin N, Wendland M, Vexler ZS, 2011. Microglial cells contribute to endogenous brain defenses after acute neonatal focal stroke. J. Neurosci 31, 12992–13001. [PubMed: 21900578]

Fernandez-Lopez D, Faustino J, Klibanov AL, Derugin N, Blanchard E, Simon F, Leib SL, Vexler ZS, 2016. Microglial cells prevent hemorrhage in neonatal focal arterial stroke. J. Neurosci 36, 2881–2893. [PubMed: 26961944]

Fitzner D, Schnaars M, van Rossum D, Krishnamoorthy G, Dibaj P, Bakhti M, Regen T, Hanisch UK, Simons M, 2011. Selective transfer of exosomes from oligodendrocytes to microglia by macropinocytosis. J. Cell Sci 124, 447–458. [PubMed: 21242314]

Fruhbeis C, Frohlich D, Kuo WP, Kramer-Albers EM, 2013. Extracellular vesicles as mediators of neuron-glia communication. Front. Cell. Neurosci 7, 182. [PubMed: 24194697]

Garner RT, Solfest JS, Nie Y, Kuang S, Stout J, Gavin TP, 2020. Multivesicular body and exosome pathway responses to acute exercise. Exp. Physiol 105, 511–521. [PubMed: 31917487]

Greening DW, Simpson RJ, 2018. Understanding extracellular vesicle diversity — current status. Expert. Rev. Proteomics 15, 887–910. [PubMed: 30326765]

Gupta A, Pulliam L, 2014. Exosomes as mediators of neuroinflammation. J. Neuroinflammation 11, 68. [PubMed: 24694258]

Gyorgy B, Hung ME, Breakefield XO, Leonard JN, 2015. Therapeutic applications of extracellular vesicles: clinical promise and open questions. Annu. Rev. Pharmacol. Toxicol 55, 439–464. [PubMed: 25292428]

Han KY, Chang JH, Azar DT, 2019. MMP14-containing exosomes cleave VEGFR1 and promote VEGFA-induced migration and proliferation of vascular endothelial cells. Invest. Ophthalmol. Vis. Sci 60, 2321–2329. [PubMed: 31117124]

Hazelton I, Yates A, Dale A, Roodselaar J, Akbar N, Ruitenberg MJ, Anthony DC, Couch Y, 2018. Exacerbation of acute traumatic brain injury by circulating extracellular vesicles. J. Neurotrauma 35, 639–651. [PubMed: 29149810]

Henne WM, Buchkovich NJ, Emr SD, 2011. The ESCRT pathway. Dev. Cell 21, 77–91. [PubMed: 21763610]

Hiltbrunner S, Larssen P, Eldh M, Martinez-Bravo MJ, Wagner AK, Karlsson MC, Gabrielsson S, 2016. Exosomal cancer immunotherapy is independent of MHC molecules on exosomes. Oncotarget 7, 38707–38717. [PubMed: 27231849]

Hughes AN, Appel B, 2020. Microglia phagocytose myelin sheaths to modify developmental myelination. Nat. Neurosci 23, 1055–1066. [PubMed: 32632287]

Kanada M, Bachmann MH, Hardy JW, Frimannson DO, Bronsart L, Wang A, Sylvester MD, Schmidt TL, Kaspar RL, Butte MJ, Matin AC, Contag CH, 2015. Differential fates of biomolecules delivered to target cells via extracellular vesicles. Proc. Natl. Acad. Sci. U. S. A 112, E1433–E1442. [PubMed: 25713383]

Karasu E, Eisenhardt SU, Harant J, Huber-Lang M, 2018. Extracellular vesicles: packages sent with complement. Front. Immunol 9, 721. [PubMed: 29696020]

Keren-Shaul H, Spinrad A, Weiner A, Matcovitch-Natan O, Dvir-Szternfeld R, Ulland TK, David E, Baruch K, Lara-Astaiso D, Toth B, Itzkovitz S, Colonna M, Schwartz M, Amit I, 2017. A unique microglia type associated with restricting development of Alzheimer's disease. Cell 169 (1276–1290), e1217.

Lai CP, Breakefield XO, 2012. Role of exosomes/microvesicles in the nervous system and use in emerging therapies. Front. Physiol 3, 228. [PubMed: 22754538]

Lawson C, Kovacs D, Finding E, Ulfelder E, Luis-Fuentes V, 2017. Extracellular vesicles: evolutionarily conserved mediators of intercellular communication. Yale J. Biol. Med 90, 481–491. [PubMed: 28955186]

Lemaire Q, Raffo-Romero A, Arab T, Van Camp C, Drago F, Forte S, Gimeno JP, Begard S, Colin M, Vizioli J, Sautière PE, Salzet M, Lefebvre C, 2019. Isolation of microglia-derived extracellular vesicles: towards miRNA signatures and neuroprotection. J. Nanobiotechnol 17, 119.

Li F, Faustino J, Woo M, Derugin N, Vexler ZS, 2015. Lack of the scavenger receptor CD36 alters microglial phenotypes after neonatal stroke. J. Neurochem 13, 445–452. 26223273.

Li J, Manickam G, Ray S, Oh CD, Yasuda H, Moffatt P, Murshed M, 2016. Smpd3 expression in both chondrocytes and osteoblasts is required for normal endochondral bone development. Mol. Cell. Biol 36, 2282–2299. [PubMed: 27325675]

Li JJ, Wang B, Kodali MC, Chen C, Kim E, Patters BJ, Lan L, Kumar S, Wang X, Yue J, Liao FF, 2018. In vivo evidence for the contribution of peripheral circulating inflammatory exosomes to neuroinflammation. J. Neuroinflammation 15, 8. [PubMed: 29310666]

Martinez-Biarge M, Ferriero DM, Cowan FM, 2019. Perinatal arterial ischemic stroke. Handb. Clin. Neurol 162, 239–266. [PubMed: 31324313]

Mrdjen D, Pavlovic A, Hartmann FJ, Schreiner B, Utz SG, Leung BP, Lelios I, Heppner FL, Kipnis J, Merkler D, Greter M, Becher B, 2018. High-dimensional single-cell mapping of central nervous system immune cells reveals distinct myeloid subsets in health, aging, and disease. Immunity 48 (380–395), e386.

Murgoci AN, Duhamel M, Raffo-Romero A, Mallah K, Aboulouard S, Lefebvre C, Kobeissy F, Fournier I, Zilkova M, Maderova D, Cizek M, Cizkova D, Salzet M, 2020. Location of neonatal microglia drives small extracellular vesicles content and biological functions in vitro. J. Extracell Vesicles 9, 1727637. [PubMed: 32158520]

Nakai W, Yoshida T, Diez D, Miyatake Y, Nishibu T, Imawaka N, Naruse K, Sadamura Y, Hanayama R, 2016. A novel affinity-based method for the isolation of highly purified extracellular vesicles. Sci. Rep 6, 33935. [PubMed: 27659060]

Norris GT, Kipnis J, 2019. Immune cells and CNS physiology: microglia and beyond. J. Exp. Med 216, 60–70. [PubMed: 30504438]

Panagiotou N, Neytchev O, Selman C, Shiels PG, 2018. Extracellular vesicles, ageing, and therapeutic interventions. Cells 7.

Paolicelli RC, Bergamini G, Rajendran L, 2019. Cell-to-cell communication by extracellular vesicles: focus on microglia. Neuroscience 405, 148–157. [PubMed: 29660443]

Paul D, Baena V, Ge S, Jiang X, Jellison ER, Kiprono T, Agalliu D, Pachter JS, 2016. Appearance of claudin-5+ leukocytes in the central nervous system during neuroinflammation: a novel role for endothelial-derived extracellular vesicles. J. Neuroinflammation 13, 292. [PubMed: 27852330]

Pérez-Boza J, Lion M, Struman I, 2018. Exploring the RNA landscape of endothelial exosomes. Rna 24, 423–435. [PubMed: 29282313]

Pulliam L, Sun B, Mustapic M, Chawla S, Kapogiannis D, 2019. Plasma neuronal exosomes serve as biomarkers of cognitive impairment in HIV infection and Alzheimer's disease. J Neurovirol. 25 (5), 702–709. 10.1007/S13365-018-0695-4. Epub 2019 Jan 4. [PubMed: 30610738]

Rajendran L, Bali J, Barr MM, Court FA, Kramer-Albers EM, Picou F, Raposo G, van der Vos KE, van Niel G, Wang J, Breakefield XO, 2014. Emerging roles of extracellular vesicles in the nervous system. J. Neurosci 34, 15482–15489. [PubMed: 25392515]

Sharma M, Naslavsky N, Caplan S, 2008. A role for EHD4 in the regulation of early endosomal transport. Traffic 9, 995–1018. [PubMed: 18331452]

Song Y, Li Z, He T, Qu M, Jiang L, Li W, Shi X, Pan J, Zhang L, Wang Y, Zhang Z, Tang Y, Yang GY, 2019. M2 microglia-derived exosomes protect the mouse brain from ischemia-reperfusion injury via exosomal miR-124. Theranostics 9, 2910–2923. [PubMed: 31244932]

Stahl PD, Raposo G, 2019. Extracellular vesicles: exosomes and microvesicles, integrators of homeostasis. Physiology (Bethesda) 34, 169–177. [PubMed: 30968753]

Stoffel W, Jenke B, Blöck B, Zumbansen M, Koebke J, 2005. Neutral sphingomyelinase 2 (smpd3) in the control of postnatal growth and development. Proc. Natl. Acad. Sci. U. S. A 102, 4554–4559. [PubMed: 15764706]

Stoffel W, Hammels I, Jenke B, Binczek E, Schmidt-Soltau I, Brodesser S, Schauss A, Etich J, Heilig J, Zaucke F, 2016. Neutral sphingomyelinase (SMPD3) deficiency disrupts the Golgi secretory pathway and causes growth inhibition. Cell Death Dis. 7, e2488. [PubMed: 27882938]

Stoffel W, Jenke B, Schmidt-Soltau I, Binczek E, Brodesser S, Hammels I, 2018. SMPD3 deficiency perturbs neuronal proteostasis and causes progressive cognitive impairment. Cell Death Dis 9, 507. [PubMed: 29725009]

Tani M, Hannun YA, 2007. Analysis of membrane topology of neutral sphingomyelinase 2. FEBS Lett. 581, 1323–1328. [PubMed: 17349629]

Tay TL, Mai D, Dautzenberg J, Fernandez-Klett F, Lin G, Sagar, Datta M, Drougard A, Stempfl T, Ardura-Fabregat A, Staszewski O, Margineanu A, Sporbert A, Steinmetz LM, Pospisilik JA, Jung S, Priller J, Grun D, Ronneberger O, Prinz M, 2017a. A new fate mapping system reveals context-dependent random or clonal expansion of microglia. Nat. Neurosci 20, 793–803. [PubMed: 28414331]

Tay TL, Savage JC, Hui CW, Bisht K, Tremblay ME, 2017b. Microglia across the lifespan: from origin to function in brain development, plasticity and cognition. J. Physiol 595, 1929–1945. [PubMed: 27104646]

Testai FD, Hillmann M, Amin-Hanjani S, Gorshkova I, Berdyshev E, Gorelick PB, Dawson G, 2012. Changes in the cerebrospinal fluid ceramide profile after subarachnoid hemorrhage. Stroke 43, 2066–2070. [PubMed: 22713492]

Tomiuk S, Zumbansen M, Stoffel W, 2000. Characterization and subcellular localization of murine and human magnesium-dependent neutral sphingomyelinase. J. Biol. Chem 275, 5710–5717. [PubMed: 10681556]

Trajkovic K, Hsu C, Chiantia S, Rajendran L, Wenzel D, Wieland F, Schwille P, Brugger B, Simons M, 2008. Ceramide triggers budding of exosome vesicles into multivesicular endosomes. Science 319, 1244–1247. [PubMed: 18309083]

Udeochu JC, Sanchez-Diaz C, Cai A, Jovicic A, Villeda SA, 2018. Exosome release promotes inflammatory resolution in activated and aged microglia. BioRxiv 10.1101/423558.

Ueno M, Fujita Y, Tanaka T, Nakamura Y, Kikuta J, Ishii M, Yamashita T, 2013. Layer V cortical neurons require microglial support for survival during postnatal development. Nat. Neurosci 16, 543–551. [PubMed: 23525041]

Verderio C, Matteoli M, 2001. ATP mediates calcium signaling between astrocytes and microglial cells: modulation by IFN-gamma. J. Immunol 166, 6383–6391. [PubMed: 11342663]

Verderio C, Muzio L, Turola E, Bergami A, Novellino L, Ruffini F, Riganti L, Corradini I, Francolini M, Garzetti L, Maiorino C, Servida F, Vercelli A, Rocca M, Dalla Libera D, Martinelli V, Comi G, Martino G, Matteoli M, Furlan R, 2012. Myeloid microvesicles are a marker and therapeutic target for neuroinflammation. Ann. Neurol 72, 610–624. [PubMed: 23109155]

Verderio C, Gabrielli M, Giussani P, 2018. Role of sphingolipids in the biogenesis and biological activity of extracellular vesicles. J. Lipid Res 59, 1325–1340. [PubMed: 29853528]

Vexler ZS, Yenari MA, 2009. Does inflammation after stroke affect the developing brain differently than adult brain? Dev. Neurosci 31, 378–393. [PubMed: 19672067]

Wacker BK, Freie AB, Perfater JL, Gidday JM, 2012. Junctional protein regulation by sphingosine kinase 2 contributes to blood-brain barrier protection in hypoxic preconditioning-induced cerebral ischemic tolerance. J. Cereb. Blood Flow Metab 32, 1014–1023. [PubMed: 22314269]

Woo MS, Wang X, Faustino J, Derugin N, Wendland MF, Zhou P, Iadecola C, Vexler ZS, 2012. Genetic deletion of CD36 enhances injury after acute neonatal stroke. Ann. Neurol 72, 961–970. . [PubMed: 23280844]

Xin H, Li Y, Chopp M, 2014. Exosomes/miRNAs as mediating cell-based therapy of stroke. Front. Cell. Neurosci 8, 377. [PubMed: 25426026]

Xu R, Greening DW, Zhu HJ, Takahashi N, Simpson RJ, 2016a. Extracellular vesicle isolation and characterization: toward clinical application. J. Clin. Invest 126, 1152–1162. [PubMed: 27035807]

Xu Y, Liu Y, Yang C, Kang L, Wang M, Hu J, He H, Song W, Tang H, 2016b. Macrophages transfer antigens to dendritic cells by releasing exosomes containing dead-cell-associated antigens partially through a ceramide-dependent pathway to enhance CD4(+) T-cell responses. Immunology 149, 157–171. [PubMed: 27278624]

Zhou W, Woodson M, Sherman MB, Neelakanta G, Sultana H, 2019. Exosomes mediate Zika virus transmission through SMPD3 neutral Sphingomyelinase in cortical neurons. Emerg. Microbes Infect 8, 307–326. [PubMed: 30866785]

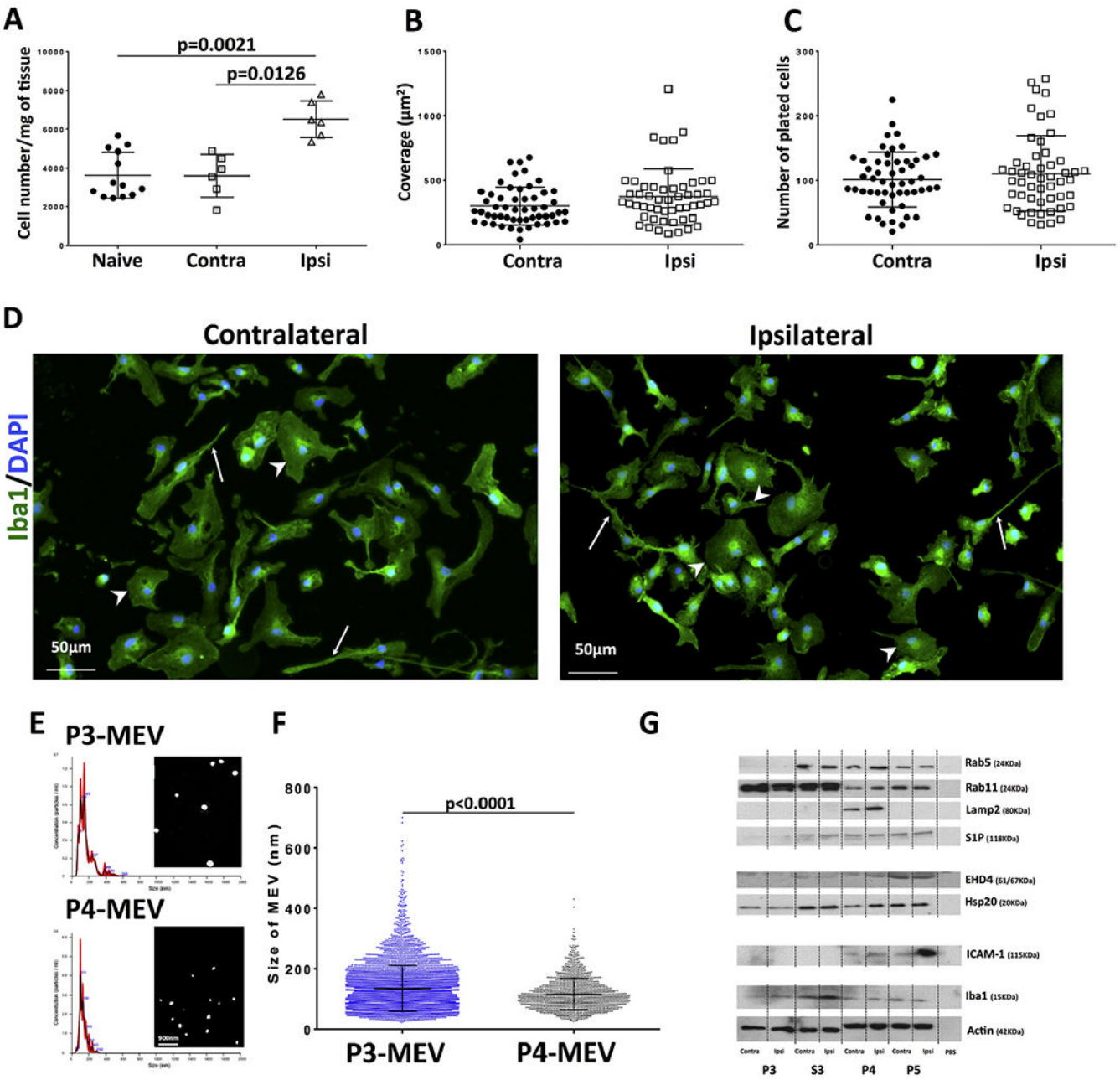

Fig. 1.

Characterization of MEV fractions derived from microglial cells isolated 24 h after tMCAO in neonatal mice. [A] The number of microglial cells pulled down by CD11b^{+}-conjugated magnetic beads from the cortex of naïve mice and from injured and matching contralateral cortex. Dots represent data from independent microglial isolations. Data are analyzed using Mann-Whitney *U* test. [B—D] Microglia from injured (Ipsi) and matching contralateral cortex (Contra) exhibit similar morphological characteristics, including similar coverage of adherent Iba1^{+} cells (B) and the number of Iba1^{+} cells (C). Each dot in B—C represents the data in individual FOV. Regardless of the source, morphology of Iba1^{+} cells is diverse and contains cells with small cell bodies and long processes (white arrow) and larger-size

cells with short processes (white arrowhead) (D). [*E*-F] Representative Nanosight images (E, right) and respective spectra (E, left) of P3-MEV and P4-MEV. The size of P4-MEV is significantly smaller than size of P3-MEV (F; $p < 0.0001$; unpaired *t*-test). [G]. Protein expression of individual EVs markers in P3-MEV, P4-MEV, P5-MEV and S3 fractions isolated from Ipsi or Contra cortex. P3 – P3-MEV; P4 – P4-MEV; P5 – P5-MEV and S3 – supernatant after step 3 centrifugation. Data are shown as mean ± SD. Statistical significance levels are as indicated on individual panels.

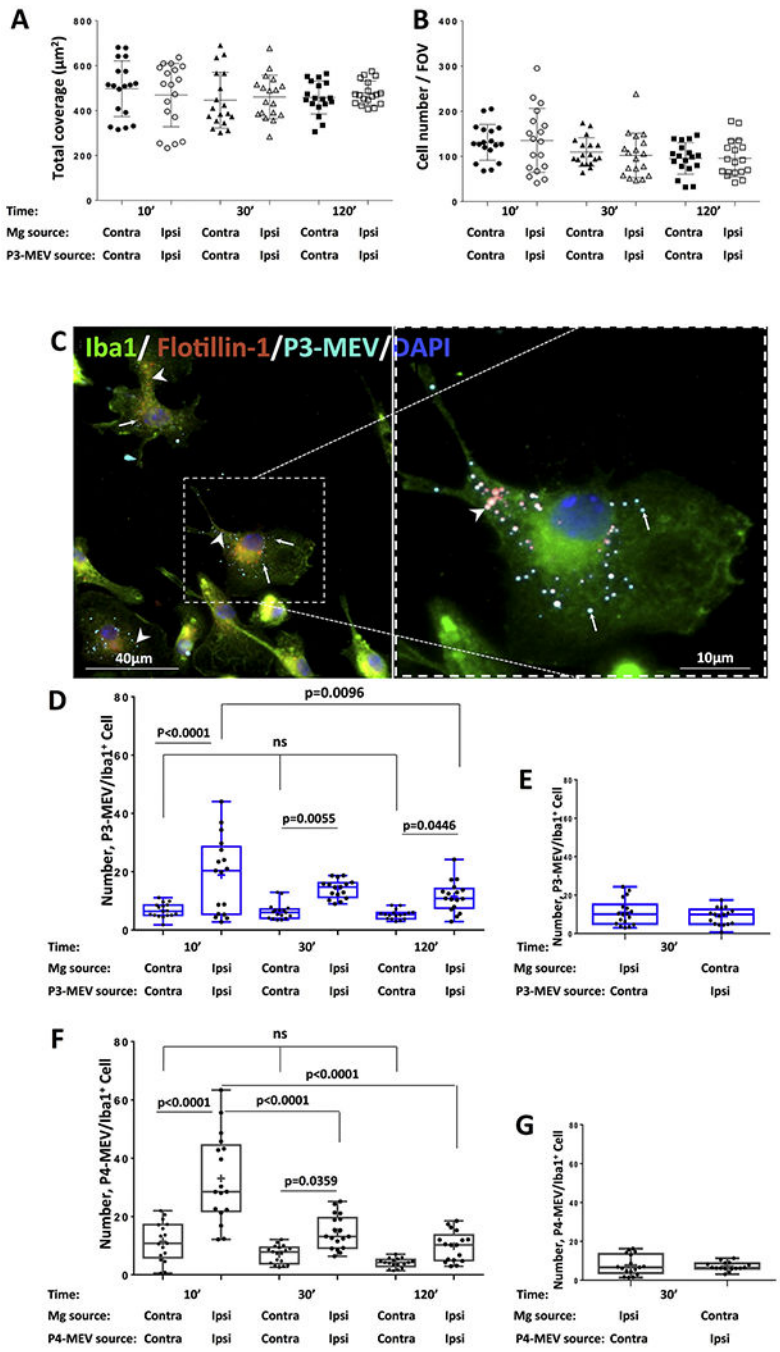

Fig. 2.

Characterization of P3-MEV and P4-MEV uptake by microglial cells isolated from injured and contralateral cortical regions 24 h after tMCAO. [A, B] Incubation of P3-MEV with cultured ^{Ipsi}-microglia or ^{Contra}-microglia for 10–120 min does not affect coverage (A) or the number (B) of microglial cells. [C] Representative image of P3-MEV^{Claret}® uptake by microglia. Note colocalization of large P3-MEV with a lipid raft protein flotillin-1. Image on the right is a cell shown in the box in image on the left. [D] Quantification of P3-MEV^{Claret}®-^{Contra}/Claret®-^{Ipsi} uptake by $^{Contra/Ipsi}$-microglia over 120 min. While

P3-MEV-$^{Claret®\text{-}Contra}$ uptake by ^{Contra}-microglia is similar over time, P3-MEV$^{Claret®\text{-}Ipsi}$ uptake is significantly increased by ^{Ipsi}-microglia ($p < 0.0001$, $p = 0.0055$, $p = 0.0446$ at three respective time points). Uptake of P3-MEV$^{Claret®\text{-}Ipsi}$ by ^{Ipsi}-microglia decreases between 10 and 120 min ($p = 0.0096$). [E] At 30 min, P3-MEV$^{Claret®\text{-}Ipsi}$ uptake by ^{Contra}-microglia and uptake of P3-MEV$^{Claret®\text{-}Contra}$ by ^{Ipsi}-microglia remain at basal levels. [F] Quantification of P4-MEV$^{Claret®}$ uptake by $^{Contra/Ipsi}$-microglia over 120 min. P4-MEV-$^{Claret®\text{-}Ipsi}$ uptake by ^{Ipsi}-microglia is significantly increased at 10 and 30 min ($p < 0.0001$, $p = 0.0359$, respectively). Uptake of P4-MEV$^{Claret®\text{-}Contra}$ by ^{Contra}-microglia remains at basal level but uptake of P4-MEV$^{Claret®\text{-}Ipsi}$ by ^{Ipsi}-microglia significantly decreases between 10 and 30 min and between 10 and 120 min ($p < 0.0001$ and $p < 0.0001$). [G] At 30 min, P4-MEV$^{Claret®\text{-}Ipsi}$ uptake by ^{Contra}-microglia and uptake of P3-MEV$^{Claret®\text{-}Contra}$ by ^{Ipsi}-microglia remain at basal levels. Data were analyzed using two-way ANOVA followed by Tukey's multiple comparisons test. Dots in D-G represent data in individual FOV. Levels of significance are as indicated on individual panels.

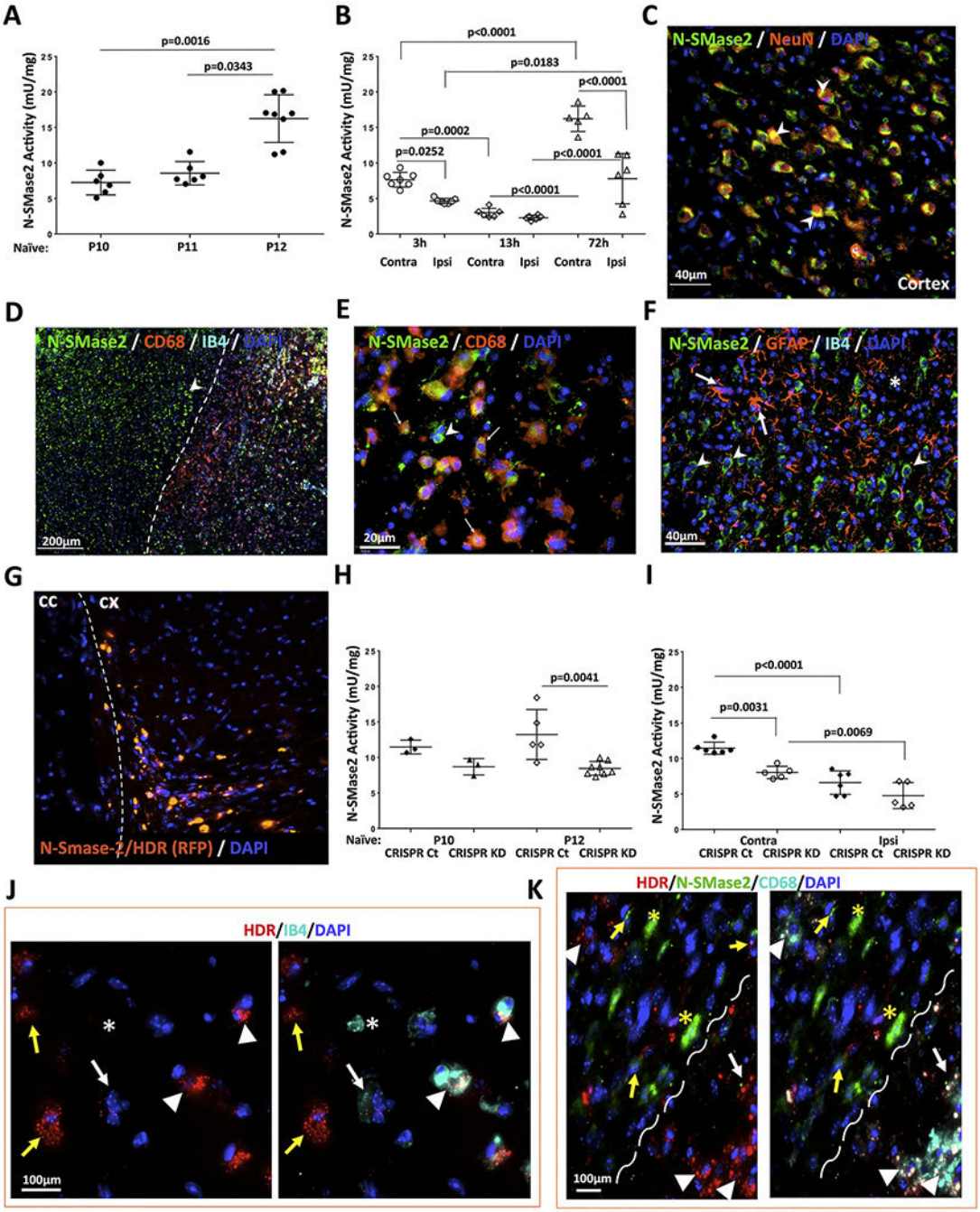

Fig. 3.

Effects of tMCAO and Smpd3 downregulation in the cortex on enzymatic activity and cell-type specific expression of N-SMase2 in neonatal brain [A]. Enzymatic activity of N-Smase2 in the cortex significantly increases between P10, P11 and P12 ($p = 0.0016$ and $p = 0.0343$ respectively; Kruskall Wallis, followed by Dunn's multiple comparisons test). [B] N-SMase2 enzymatic activity is significantly decreased in injured region 3 and 72 h after tMCAO ($p = 0.0252$ and $p < 0.0001$, respectively). N-SMase2 enzymatic activity in contralateral cortex decreases from 3 h to 13 h after reperfusion ($p = 0.0002$) while it

increases at 72 h after reperfusion, compare to 3 h ($p < 0.0001$) and 13 h ($p < 0.0001$). In Ipsilateral cortex, at 72 h after reperfusion, the N-SMase2 activity significantly increased from 3 h and 13 h post reperfusion ($p = 0.0183$ and $p < 0.0001$ respectively; two-way ANOVA followed by Tukey's multiple comparisons test). [C] N-Smase2 is expressed in $NeuN^+$ neurons (white arrowhead) in naïve brain. [D—F] N-SMase2 expression in injured and uninjured regions 72 h after tMCAO. Punctate line points to a borderline between peri-focal region and morphologically intact cortical region. Note that N-SMase2 is abundantly expressed in uninjured region in cells morphologically resembling neurons (D,F; white arrowheads), whereas in injured cortical region expression is increased in $CD68^+$ microglia/macrophages (D-E; white arrows). In E, thin arrow points to N-$SMase2^+$/$CD68^+$ cells; arrowhead point to N-$SMase2^+$ cells of non-monocyte origin. [F] There is no apparent N-SMase2 expression in $GFAP^+$ astrocytes (white arrows) located adjacent to a region with extensive cell death (* points to shrunken and irregularly-shaped $DAPI^+$ nuclei, while N-SMase2 is expressed in cells morphologically resembling neurons (white arrowheads; F). [G] Visualization of intracortical injection site using Smpd3/Ct-HDR^{RFP+} plasmid. [H] Intra-cerebral injection of CRISPR-Cas9/KO-HDR plasmid (Smdp3/KD) at P7 leads to downregulation of Smpd3 and significant decrease of N-SMase2 activity at P12 in naïve mice (H, $p = 0.0041$) as well as in contralateral ($p = 0.0031$) and, further, in injured cortex 72 h after tMCAO (I, $p = 0.0069$; Kruskall Wallis followed by Dunn's multiple comparisons test). [I] Decrease of N-SMase2 activity is more profound in ipsilateral cortex after P7 Smpd3/Ct-HDR plasmid administration ($p < 0.0001$; two-way ANOVA followed by a Tukey's multiple comparisons test). [J] Immunofluorescence tracking of the distribution of HDR, which was injected together with plasmid, demonstrates high (arrowheads) and more modest HDR expression (white thin arrow) in $IB4^+$ cells in injured cortex in Smpd3/KD-HDR treated mice 24 h after reperfusion. Few $IB4^+$ cells show no detectible HDR level (asterisk). HDR is also present in $IB4^-$ cells (yellow arrows). [K] Visualization of N-SMase2 expression in peri-focal region and in morphologically intact cortical region of Smpd3/KD-HDR mice (regions delineated by discontinued white line) 72 h after reperfusion. Arrowheads indicate HDR in N-$SMase2^-$/$CD68^+$ cells. Yellow arrows indicate diminished N-SMase2 expression in HDR^+ cells in morphologically intact zone. Yellow asterisk indicates high N-SMase2 expression in HDR^- cells. Abbreviations: cc: corpus callosum, cx: cortex, Contra: contralateral, Ipsi: injured. Shown are mean ± SD. Dots in A, B, H and I represent data from individual mice. Levels of significance are as indicated on individual panels. (For interpretation of the references to colour in this figure legend, the reader is referred to the web version of this article.)

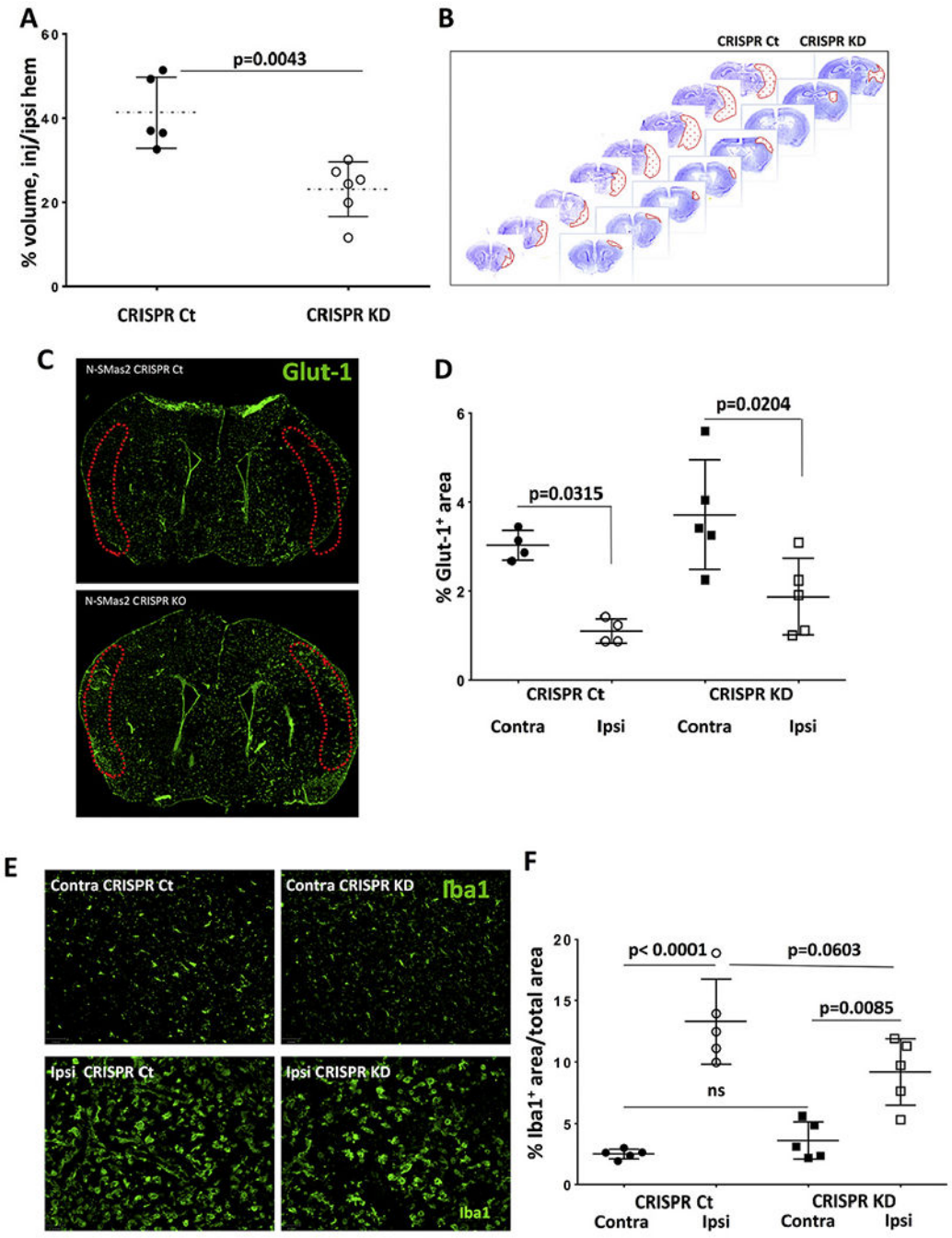

Fig. 4.

Effect of Smpd3 downregulation in the cortex on injury volume, vessel coverage and microglial activation 72 h after tMCAO. [A] Compared to that in Smpd3/Ct mice, injury volume is significantly decreased in Smpd3/KD mice ($p = 0.0043$; Mann Whitney test). [B] Representative examples of anterior-to-posterior coronal sections stained with cresyl violet; injury zone is defined in red. [C—D] Representative low magnification images of Glut-1$^+$ vessel coverage in brains of Smpd3/Ct (C, top) and Smpd3/KD (C, bottom) mice. Quantification of vessel coverage in the cortex in D was performed in areas demarcated

with punctate boundaries. Vessel coverage is significantly decreased in ischemic-reperfused regions in Smpd3/Ct ($p = 0.0315$) and Smpd3/KD ($p = 0.0204$) mice, with no difference between groups. [E, F] Iba1$^+$ coverage/FOV is significantly increased in injured compared to that in contralateral regions ($p < 0.0001$ in Smpd3/Ct and $p = 0.0085$ in Smpd3/KD). Increase was less profound in ipsilateral cortex in Smpd3/KD pups. In E, F, differences were analyzed using two-way ANOVA followed by Tukey's multiple comparisons test. Levels of significance are as indicated on individual panels. (For interpretation of the references to colour in this figure legend, the reader is referred to the web version of this article.)

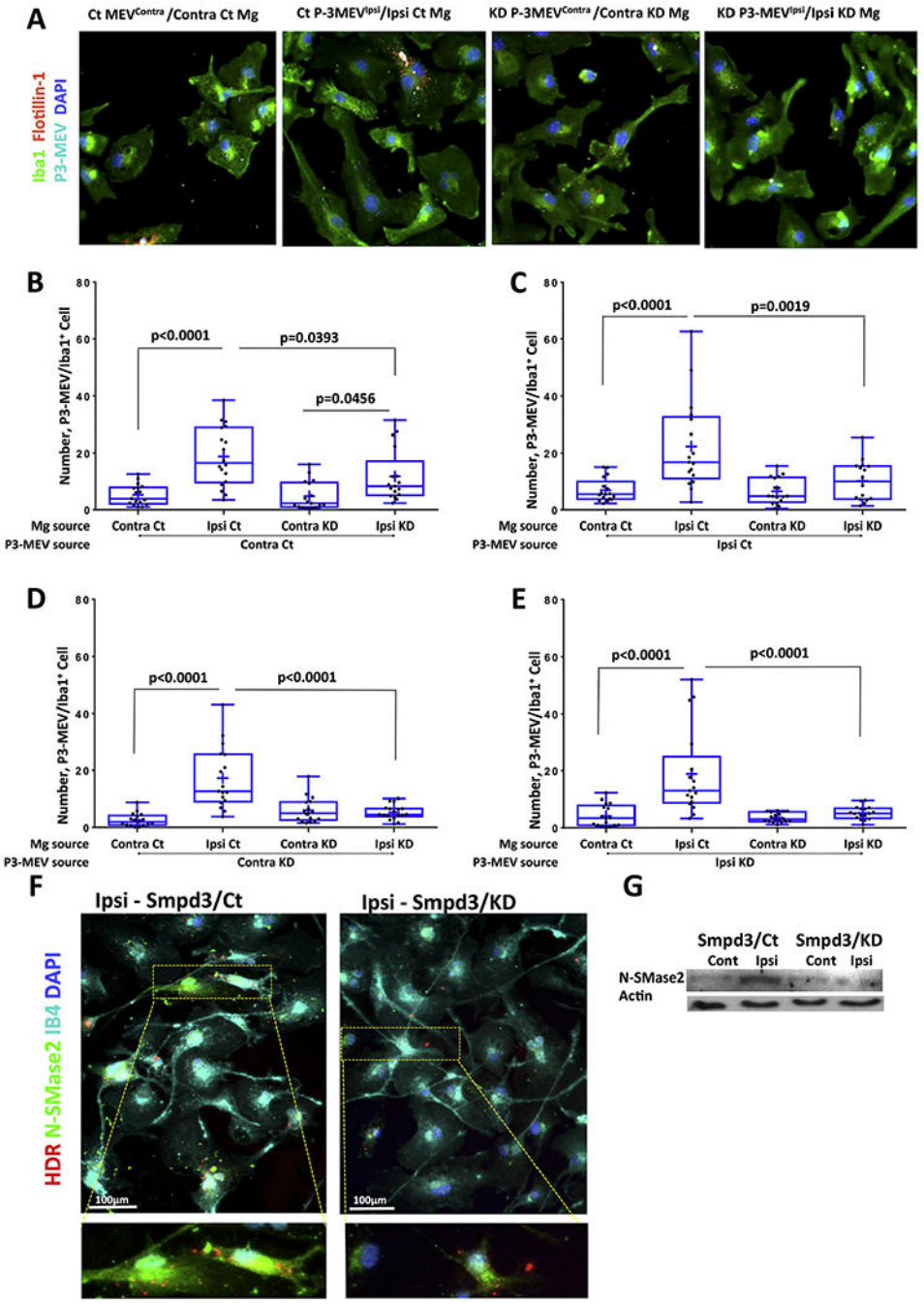

Fig. 5.

Effects of *Smpd3* gene downregulation in the cortex on P3-MEV uptake by microglial cells isolated from injured and uninjured cortex 72 h after tMCAO. [A] Representative images of Iba1^{+} cells isolated from Smpd3/Ct or Smpd3/KD mice. [B] P3-MEV$^{\text{Claret®-Contra}}$ uptake from Smpd3/Ct by $^{\text{Ipsi-}}$microglia from Smpd3/Ct and Smpd3/KD mice is significantly increased ($p < 0.000$ and $p = 0.0456$, respectively). The uptake is significantly attenuated by $^{\text{Ipsi-}}$microglia from Smpd3/KD ($p = 0.0393$). [C] Uptake of P3-MEV$^{\text{Claret®-Ipsi}}$ from Smpd3/Ct is significantly increased by $^{\text{Ipsi-}}$microglia from Smpd3/Ct ($p < 0.0001$) but

not from Smpd3/KD mice. The latest is decreased by microglia from Smpd3/KD mice. The uptake is significantly attenuated by $^{Ipsi-}$microglia from Smpd3/KD ($p = 0.0019$). [D] Uptake of P3-MEV$^{Claret®-Contra}$ from Smpd3/KD is significantly increased by $^{Ipsi-}$microglia from Smpd3/Ct ($p < 0.0001$) but is abolished by microglia from Smpd3/KD mice. The uptake is significantly attenuated by $^{Ipsi-}$microglia from Smpd3/KD ($p < 0.0001$). [E] P3-MEV$^{Claret®-Ipsi}$ uptake is significantly increased by $^{Ipsi-}$microglia from Smpd3/Ct ($p \leq 0.0001$) but is abolished by $^{Ipsi-}$microglia from Smpd3/KD ($p < 0.0001$). In B-E, two-way ANOVA followed by Tukey's multiple comparisons test was used. Levels of significance are as indicated on individual panels. [F] Immunofluorescence images of HDR$^+$/N-SMase2$^+$/IB4$^+$ microglial cells from injured regions of Smpd3/Ct (left) and Smpd3/KD (right) pups. Note the presence of HDR$^+$ and abundance of N-SMase2$^+$ cells in Smpd3/Ct microglia but lower or lack of N-SMase2$^+$ expression in HDR$^+$ cells from and Smpd3/KD pups. Two respective higher magnification HDR$^+$/N-SMase2$^+$ images from boxes in (F) are shown below. [G] Western Blot demonstrating N-SMase2 expression in microglia lysed after collecting supernatants for MEV isolation.

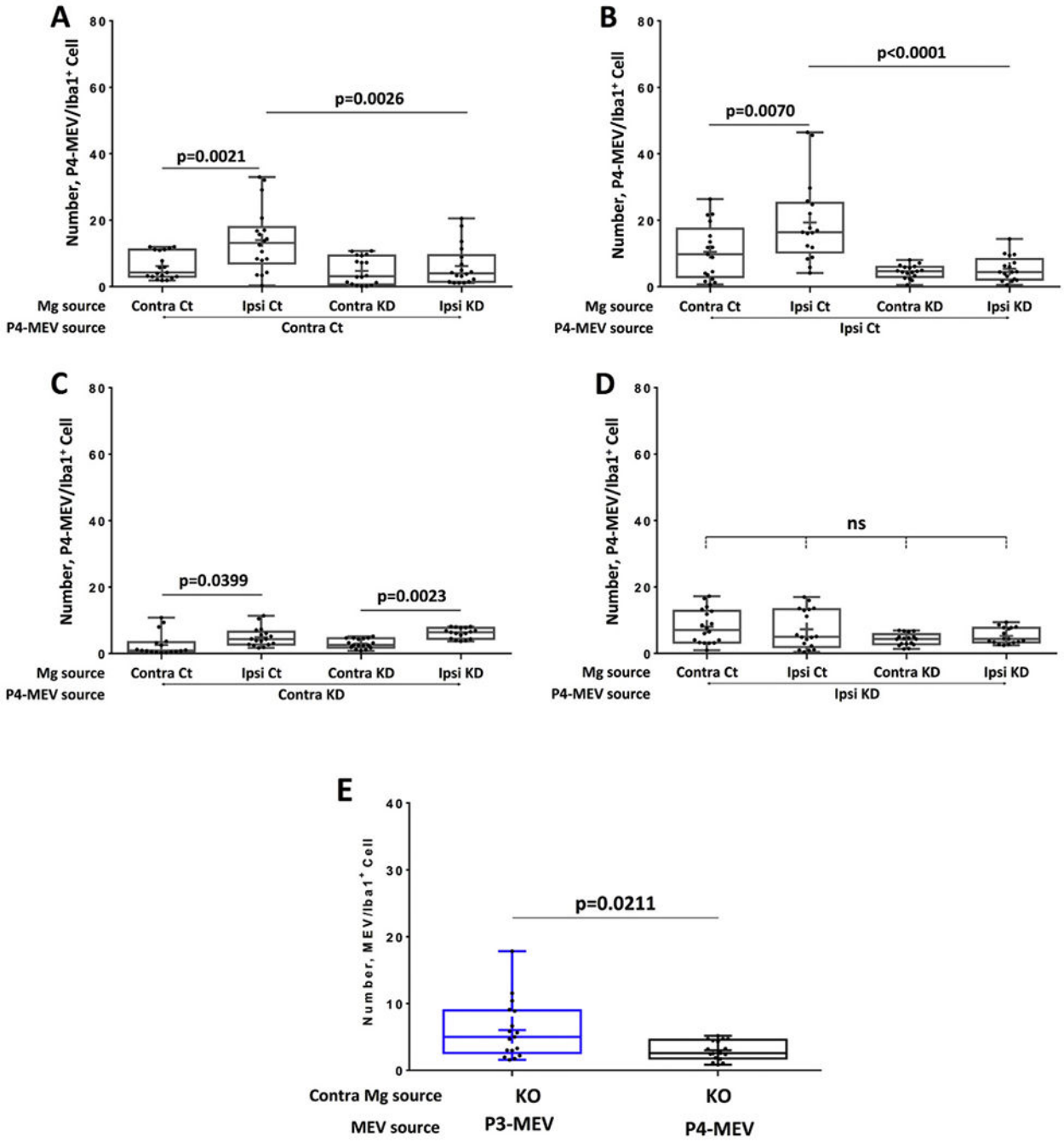

Fig. 6.

Effect of Smpd3 downregulation in the cortex on uptake of P4-MEV by microglia isolated 24 h after tMCAO. [A-B] Uptake of P4-MEV$^{Claret®\text{-}Contra}$ (A) and P4-MEV$^{Claret®\text{-}Ipsi}$ (B) from Smpd3/Ct by Smpd3/KD $^{Contra/Ipsi}$-microglia is significantly increase compared to uptake by Smpd3/Ct ^{Contra}-microglia ($p = 0.0021$ and $p = 0.0070$, respectively). Uptake of P4-MEV$^{Claret®\text{-}Contra}$ (A) and P4-MEV$^{Claret®\text{-}Ipsi}$ (B) from Smpd3/Ct by Smpd3/KD $^{Contra/Ipsi}$-microglia is significantly decreased compared to uptake by Smpd3/Ct ^{Ipsi}-microglia ($p = 0.0026$ and $p < 0.0001$, respectively). [C] A small but significant increase

in uptake of P4-MEV$^{Claret®\text{-}Contra}$ from Smpd3/KD by microglia Smpd3/Ct-^{Ipsi} and Smpd3/KD-^{Ipsi} ($p = 0.0399$ and $p = 0.0023$ respectively). [D] P4-MEV$^{Claret®\text{-}Ipsi}$ uptake from Smpd3/KD is similar regardless of microglial source. Differences between four groups in A-D were analyzed using two-way ANOVA followed by Tukey's multiple comparisons test. [E] The number of P4-MEV$^{Claret®}$ per Smpd3/KD-^{Contra} microglial cell is significantly lower than the number of P3-MEV$^{Claret®}$ ($p = 0.0211$; Mann Whitney test).